A frequency- and intensity-dependent macroelement for reduced order seismic analysis of soil-structure interacting systems

Nikolaos Lesgidis[1], Anastasios Sextos[1,2*] and Oh-Sung Kwon[3]
[1] *Department of Civil Engineering, Aristotle University Thessaloniki, Greece*
[2] *Department of Civil Engineering, University of Bristol, United Kingdom*
[3] *Department of Civil Engineering, University of Toronto, Canada*
[*] corresponding author

SUMMARY

The computational demand of the soil-structure interaction (SSI) analysis for the design and assessment of structures, as well as for the evaluation of their life-cycle cost and risk exposure has led the civil engineering community to the development of a variety of methods towards the model order reduction of the coupled soil-structure dynamic system in earthquake regions. Different approaches have been proposed in the past as computationally efficient alternatives to the conventional FEM simulation of the complete soil-structure domain, such as the nonlinear lumped spring, the macroelement method and the substructure partition method. Yet no approach was capable of capturing simultaneously the frequency-dependent dynamic properties along with the nonlinear behavior of the condensed segment of the overall soil-structure system under strong earthquake ground motion, thus generating an imbalance between the modeling refinement achieved for the soil and the structure. To this end, a dual frequency- and intensity-dependent expansion of the Lumped Parameter Modeling method is proposed in the current paper, materialized through a multi-objective algorithm, capable of closely approximating the behavior of the nonlinear dynamic system of the condensed segment. This is essentially the extension of an established methodology, also developed by the authors, in the inelastic domain. The efficiency of the proposed methodology is validated for the case of a bridge foundation system, wherein the seismic response is comparatively assessed for both the proposed method and the detailed finite element model. The above expansion is deemed a computationally efficient and reliable method for simultaneously considering the frequency and amplitude dependence of soil-foundation systems in the framework of nonlinear seismic analysis of SSI systems.

Keywords: soil-structure interaction, macroelement, model order reduction, Lumped Parameter Model

1. INTRODUCTION

As has been observed in multiple occasions in the past [1], the supporting soil can play an essential role on the behavior of a superstructure during strong earthquake ground shaking. The soil–structure interaction effect under such a hazard can lead to unexpected structural behavior, which cannot be easily predicted in advance. As a result, a realistic representation of the semi-infinite soil domain during the simulation of the soil-structure interacting system is considered an essential prerequisite for an accurate dynamic analysis and seismic performance prediction.

Numerous approaches have been established in the past addressing the modelling of the soil-structure interaction from several different perspectives. The truncated soil domain finite element method is an example of a direct approach for the simulation of the aforementioned effect, where a detailed behavior of the soil-foundation system, including material and geometrical complexity, can be obtained. The truncated Finite element method has been implemented in multiple occasions for the seismic analysis of a soil-bridge system [2–4]. However, such an approach can be computationally demanding for the analysis of complex structures to such an extent, that it is almost prohibitive, particularly in the framework of probabilistic assessment that requires a large number of model realizations and analyses.

In the light of the above limitations, the most common approach is to sacrifice the modeling refinement in terms of subsoil domain size and the subsequent analysis accuracy by reducing the order of the system. Primary focus is then made on refined models that are tailored to capture seismic damage at specific structural and foundation components. Particularly for bridge structures, geometric nonlinearities that may arise from gap (i.e., joint) closure, abutment ratcheting and stopper activation during strong ground motion are also taken into consideration as they instantaneously affect the boundary conditions. Such a task can be accomplished through a partition

approach of the overall dynamic system in segments, where the domain of the soil and foundation is significantly condensed on its internal degrees of freedom (DOF) or completely replaced by a simplified representation, while the superstructure is left unaltered. Numerous implementations on the substructure modeling approach have been proposed in the past, among which the macroelement method stands out as an effective tool capable of coping with complex constitutive laws and geometrical nonlinearities.

The latter macroelement approach is a concept initially introduced by Montrasio et al [5], and further developed by a number of different research groups [6–11], that has successfully provided with an accurate, yet computationally efficient, representation of both the elastic and inelastic cyclic behavior of the soil-foundation domain. The main challenge with this approach is that, although it emulates with great detail the different mechanisms triggered during a quasi-static excited simulation, quite commonly oversimplifies or even completely neglects the dynamic traits of the foundation soil domain through the use of complementary Kelvin –Voigt components. As these components are only accurate at a specific target (i.e., commonly the predominant) frequency of seismic excitation, their use can lead to significant error on their seismic response, as illustrated in [12] for the case of bridges resting of various soil profiles.

A successful attempt to incorporate the frequency dependence in macroelements has been recently made by Chai et al [13]. However, as the proposed method is mainly focused on the frequency dependent traits of the system in the elastic domain, oscillations in higher intensity and high-frequency regions are represented by unexplored dynamic properties, thus suggesting potential misrepresentation of the soil foundation domain under the aforementioned circumstances.

To address the above limitations, a frequency-dependent macroelement method with emulated dynamic properties across various levels of increasing seismic intensity is proposed in the current study. The viscoelastic dynamic properties of the soil foundation domain along a broad frequency spectrum are successfully emulated in the time domain through the use of the Lumped Parameter Modeling method [14–17] based on the method's documented success in the elastic range, to preserve the original system's accuracy, stability and passivity.

Along these lines, more specific objectives of the present study are: (a) to extend the method proposed by the authors for considering the frequency-dependence of soil-structure interaction in the context of seismic analysis of SSI systems in the time domain by further developing the required extraction technique, capable of selecting representative properties of the dynamic soil-structure system over different intensity levels; and (b) to verify numerically, the proposed procedure by means of a single DOF bridge model subjected to earthquake loading. The model formulation as well as the verification examples are reported in the following.

2. INELASTIC SSI SYSTEM ORDER REDUCTION

An essential step towards the expansion of the macroelement method to inelastic frequency dependent systems is the derivation of representative dynamic properties of the system in different levels of excitation intensity. The concept of the frequency domain generated impedance function has been proven to efficiently emulate the behaviour of a viscous-elastic system for a selected interface region. However the concept of the impedance function cannot be directly applied in inelastic dynamic systems. A dynamic trait extraction approach for inelastic dynamic systems is presented in the following paragraphs, implementing the linearization and dynamic condensation of the soil –foundation segment of the overall SSI system.

2.1 System Linearization on a selected Variables State

The mathematical representation of the superstructure – foundation – semi-infinite soil domain system can be illustrated in the classic ODE (Ordinary Differential Equation) formulation of equation (1) after the appropriate geometrical discretization of the original PDE equation system.

$$\mathbf{M}\ddot{\mathbf{u}} + \mathbf{C}\dot{\mathbf{u}} + \mathbf{f}(\mathbf{u},\boldsymbol{\alpha}) = \mathbf{F}$$

$$\mathbf{H}(\boldsymbol{\alpha},\mathbf{u}) = \mathbf{0} \tag{1}$$

The variables **M** and **C** denote the mass and damping coefficient matrices of the system, **f(u,α)** denotes the nonlinear force to displacement relation vector while **F** is the external loading vector applied to the respective DOFs. Vector **u** denotes the displacement of the system DOFs, vector **α** represents the internal variables defining the inelastic behavior of **f(u,α)** while **H(α,u)** are the functions governing the evolution of the internal variable vector **α**. As previously discussed, only the soil foundation segment is targeted by the order reduction approach, while the superstructure segment is left intact. As a result, the overall system is partitioned into individual segments according to the substructure partition method illustrated in Figure 1.

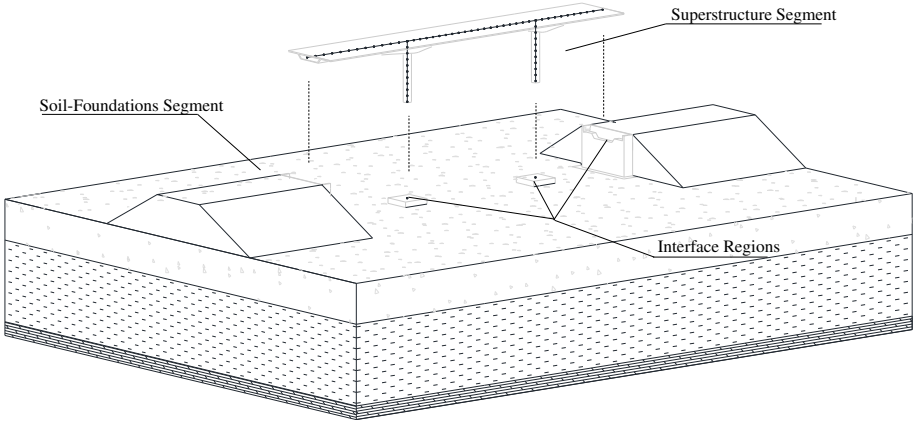

Figure 1. SSI system partition through substructure method

$$, \quad \mathbf{M}=\begin{bmatrix} \mathbf{M}_{ss,ss} & \mathbf{0} & \mathbf{0} \\ \mathbf{0} & \mathbf{M}_{i,i}^{ss}+\mathbf{M}_{i,i}^{soil} & \mathbf{0} \\ \mathbf{0} & \mathbf{0} & \mathbf{M}_{soil,soil} \end{bmatrix}, \quad \mathbf{C}=\begin{bmatrix} \mathbf{C}_{ss,ss} & \mathbf{C}_{ss,i} & \mathbf{0} \\ \mathbf{C}_{i,ss} & \mathbf{C}_{i,i}^{ss}+\mathbf{C}_{i,i}^{soil} & \mathbf{C}_{i,soil} \\ \mathbf{0} & \mathbf{C}_{soil,i} & \mathbf{C}_{soil,soil} \end{bmatrix}, \quad \mathbf{u}=\begin{bmatrix} \mathbf{u}_{ss} \\ \mathbf{u}_{i} \\ \mathbf{u}_{soil} \end{bmatrix}, \quad \mathbf{F}=\begin{bmatrix} \mathbf{F}_{ss} \\ \mathbf{F}_{i} \\ 0 \end{bmatrix}$$

$$\mathbf{f}(\mathbf{u})=\begin{bmatrix} \mathbf{f}_{ss}(\mathbf{u}_{ss},\mathbf{u}_{i},\boldsymbol{\alpha}_{ss}) \\ \mathbf{f}_{i}^{ss}(\mathbf{u}_{ss},\mathbf{u}_{i},\boldsymbol{\alpha}_{ss})+\mathbf{f}_{i}^{soil}(\mathbf{u}_{i},\mathbf{u}_{soil},\boldsymbol{\alpha}_{soil}) \\ \mathbf{f}_{soil}(\mathbf{u}_{i},\mathbf{u}_{soil},\boldsymbol{\alpha}_{soil}) \end{bmatrix}, \quad \begin{bmatrix} \mathbf{H}_{ss}(\mathbf{u}_{ss},\mathbf{u}_{i},\boldsymbol{\alpha}_{ss}) \\ \mathbf{H}_{soil}(\mathbf{u}_{i},\mathbf{u}_{soil},\boldsymbol{\alpha}_{soil}) \end{bmatrix}=\mathbf{0} \tag{2}$$

The overall system's partitions are notated with the subscript *ss*, *i soil*, and corresponding to the superstructure segment, the interface and the soil-domain - foundation segment DOFs, respectively. The dynamic system of equation (1) is expanded according to the selected segmentation as illustrated in equation (2). In the aforementioned equation, subscripts denote the segment where the DOF is located, while the superscripts used only on the interface DOF terms denote the segment from which the contributing restoring force term is originating. Through the expansion of the system of equations to its segmented form, the equation terms corresponding to the soil foundation segment are now designated, concerning both the interface and soil foundation DOFs.

The order reduction process of the soil foundation segment is initiated through the selection of a number of *"o"* representative variable states of the soil foundation segment displacements $\mathbf{u_o}=[\mathbf{u}_{i,o},\mathbf{u}_{soil,o}]^{\mathbf{T}}$ and internal plastic variables $\boldsymbol{\alpha}_{\mathbf{o}}$. For sufficiently small trajectories around each selected variable state $\mathbf{s_o}=[\mathbf{u_o}, \boldsymbol{\alpha}_{\mathbf{o}}]^{\mathbf{T}}$ a linearized version of the inelastic soil foundation segment is considered an accurate representation of the segment. Thus, for each preselected variable state $\mathbf{s_o}$, it is possible to perform a linearization process to the targeted inelastic dynamic system through the use of a 1st order Taylor expansion of the multivariable function, and proceed with the appropriate dynamic traits extraction in the frequency domain. The 1st order Taylor expansion notation is illustrated in equation (3) for the approximation of the vector valued function **f(x)** around a given vector $\mathbf{x_o}$. The symbol $\nabla_{\mathbf{x}}$ corresponds to the gradient of a vector valued function with respect to the variable vector **x**, while *M* and *N* is the length of the vector valued function *f* and vector *x* respectively.

$$\mathbf{f}(\mathbf{x}) \approx \mathbf{f}(\mathbf{x_o})+(\mathbf{x}-\mathbf{x_o})\cdot\nabla_{\mathbf{x}}\mathbf{f}(\mathbf{x_o})$$

$$\text{Where} \quad \nabla_{\mathbf{x}}\mathbf{f}(\mathbf{x_o})=\begin{bmatrix} \frac{\partial f_1(\mathbf{x_o})}{\partial x_1} & \cdots & \frac{\partial f_1(\mathbf{x_o})}{\partial x_N} \\ \vdots & \ddots & \vdots \\ \frac{\partial f_M(\mathbf{x_o})}{\partial x_1} & \cdots & \frac{\partial f_M(\mathbf{x_o})}{\partial x_N} \end{bmatrix}, \quad \mathbf{f}(\mathbf{x})=\begin{bmatrix} f_1(\mathbf{x}) \\ \vdots \\ f_M(\mathbf{x}) \end{bmatrix}, \quad \mathbf{x}=\begin{bmatrix} x_1 \\ \vdots \\ x_N \end{bmatrix} \tag{3}$$

The linearization process of the soil-foundation segment is depicted in equation (4). The nonlinear restoring force terms of the condensed segment, $\mathbf{f}_i^{soil}$ and $\mathbf{f}_{soil}$, are replaced with their representative 1st order Taylor expansion at a selected variable state $\mathbf{s_o}=[\mathbf{u}_o, \boldsymbol{\alpha}_o]^T$ where $\mathbf{u}_o=[\mathbf{u}_{i,o},\mathbf{u}_{soil,o}]^T$ and $\boldsymbol{\alpha}_o=\boldsymbol{\alpha}_{soil,o}$.

$$\mathbf{f}_{lin}(\mathbf{u})=\begin{bmatrix}\mathbf{f}_{ss}(\mathbf{u}_{ss},\mathbf{u}_i,\boldsymbol{\alpha}_{ss})\\ \mathbf{f}_i^{ss}(\mathbf{u}_{ss},\mathbf{u}_i,\boldsymbol{\alpha}_{ss})\\ \mathbf{0}\end{bmatrix}+\begin{bmatrix}\mathbf{0} & \mathbf{0} & \mathbf{0}\\ \mathbf{0} & \nabla_{\mathbf{u}_i}\mathbf{f}_i^{soil}(\mathbf{u}_o,\boldsymbol{\alpha}_o) & \nabla_{\mathbf{u}_{soil}}\mathbf{f}_i^{soil}(\mathbf{u}_o,\boldsymbol{\alpha}_o)\\ \mathbf{0} & \nabla_{\mathbf{u}_i}\mathbf{f}_{soil}(\mathbf{u}_o,\boldsymbol{\alpha}_o) & \nabla_{\mathbf{u}_{soil}}\mathbf{f}_{soil}(\mathbf{u}_o,\boldsymbol{\alpha}_o)\end{bmatrix}\cdot\begin{bmatrix}\mathbf{u}_{ss}\\ \mathbf{u}_i\\ \mathbf{u}_{soil}\end{bmatrix}+\begin{bmatrix}0\\ \mathbf{X}_i\\ \mathbf{X}_{soil}\end{bmatrix}$$

$$\mathbf{X}_i=\mathbf{f}_i^{soil}(\mathbf{u}_o,\boldsymbol{\alpha}_o)-\nabla_{\mathbf{u}_i}\mathbf{f}_i^{soil}(\mathbf{u}_o,\boldsymbol{\alpha}_o)\cdot\mathbf{u}_{i,o}-\nabla_{\mathbf{u}_{soil}}\mathbf{f}_i^{soil}(\mathbf{u}_o,\boldsymbol{\alpha}_o)\cdot\mathbf{u}_{soil,o}$$

$$\mathbf{X}_{soil}=\mathbf{f}_{soil}(\mathbf{u}_o,\boldsymbol{\alpha}_o)-\nabla_{\mathbf{u}_i}\mathbf{f}_{soil}(\mathbf{u}_o,\boldsymbol{\alpha}_o)\cdot\mathbf{u}_{i,o}-\nabla_{\mathbf{u}_{soil}}\mathbf{f}_{soil}(\mathbf{u}_o,\boldsymbol{\alpha}_o)\cdot\mathbf{u}_{soil,o} \quad (4)$$

The variable state and segment-specific linearized dynamic system can now be expanded into equations (5-7), where the terms corresponding to internal soil-foundation segment DOFs are transformed in the frequency domain as follows:

$$\mathbf{M}_{ss,ss}\ddot{\mathbf{u}}_{ss}+\mathbf{C}_{ss,ss}\dot{\mathbf{u}}_{ss}+\mathbf{C}_{ss,i}\dot{\mathbf{u}}_i+\mathbf{f}_{ss}(\mathbf{u}_{ss},\mathbf{u}_i,\boldsymbol{\alpha}_{ss})=\mathbf{F}_{ss} \quad (5)$$

$$\begin{aligned}\mathcal{F}^{-1}\{\mathcal{F}[&\mathbf{M}_{i,i}^{soil}\ddot{\mathbf{u}}_i+\mathbf{C}_{i,i}^{soil}\dot{\mathbf{u}}_i+\nabla_{\mathbf{u}_i}\mathbf{f}_i^{soil}(\mathbf{u}_o,\boldsymbol{\alpha}_o)\cdot\mathbf{u}_i+\mathbf{C}_{i,soil}\dot{\mathbf{u}}_{soil}+\nabla_{\mathbf{u}_{soil}}\mathbf{f}_i^{soil}(\mathbf{u}_o,\boldsymbol{\alpha}_o)\cdot\mathbf{u}_{soil}\\ &+\mathbf{X}_i(\mathbf{u}_o,\boldsymbol{\alpha}_o)]\}+\mathbf{M}_{i,i}^{ss}\ddot{\mathbf{u}}_i+\mathbf{C}_{i,i}^{ss}\dot{\mathbf{u}}_i+\mathbf{f}_i^{ss}(\mathbf{u}_{ss},\mathbf{u}_i,\boldsymbol{\alpha}_{ss})+\mathbf{C}_{i,ss}\dot{\mathbf{u}}_{ss}=\mathbf{F}_i\end{aligned} \quad (6)$$

$$\begin{aligned}\mathcal{F}[&\mathbf{M}_{soil,soil}\ddot{\mathbf{u}}_{soil}+\mathbf{C}_{soil,i}\dot{\mathbf{u}}_i+\mathbf{C}_{soil,soil}\dot{\mathbf{u}}_{soil}+\nabla_{\mathbf{u}_i}\mathbf{f}_{soil}(\mathbf{u}_o,\boldsymbol{\alpha}_o)\cdot\mathbf{u}_i\\ &+\nabla_{\mathbf{u}_{soil}}\mathbf{f}_{soil}(\mathbf{u}_o,\boldsymbol{\alpha}_o)\cdot\mathbf{u}_{soil}+\mathbf{X}_{soil}(\mathbf{u}_o,\boldsymbol{\alpha}_o)]=\mathbf{0}\end{aligned} \quad (7)$$

The notations $\mathcal{F}$ and $\mathcal{F}^{-1}$ denote the Fourier and the inverse Fourier transformation, respectively. Through the implementation of the designated transformations, Equations 6 and 7 can take the form of Equations 8 and 9 respectively. $\mathbf{S}_{k,l}$ represents the current variable state impedance notation $-\mathbf{M}_{k,l}\omega^2+\mathbf{C}_{k,l}\omega i+\nabla_{\mathbf{u}_l}\mathbf{f}_k(\mathbf{u}_o,\boldsymbol{\alpha}_o)$, Function $\delta(\omega)$ corresponds to the Dirac delta function, notation ,while $\mathbf{U}_j=\mathcal{F}(\mathbf{u}_j)$.

$$\mathbf{M}_{i,i}^{ss}\ddot{\mathbf{u}}_i+\mathbf{C}_{i,i}^{ss}\dot{\mathbf{u}}_i+\mathbf{C}_{i,ss}\dot{\mathbf{u}}_{ss}+\mathbf{f}_i^{ss}(\mathbf{u}_{ss},\mathbf{u}_i,\boldsymbol{\alpha}_{ss})+\mathcal{F}^{-1}\left(\mathbf{S}_{i,i}^{soil}\mathbf{U}_i+\mathbf{S}_{i,soil}\mathbf{U}_{soil}+\mathbf{X}_i(\mathbf{u}_o)\cdot2\pi\cdot\delta(\omega)\right)=\mathbf{F}_i \quad (8)$$

$$\mathbf{S}_{soil,soil}\mathbf{U}_{soil}+\mathbf{S}_{soil,i}\mathbf{U}_i+\mathbf{X}_{soil}(\mathbf{u}_o,\boldsymbol{\alpha}_o)\cdot2\pi\cdot\delta(\omega)=0 \quad (9)$$

The dynamic system of equations (4) can now be significantly reduced in size through the elimination of the soil foundation segment internal DOFs $\mathbf{u}_{soil}$:

$$\mathbf{M}\cdot\ddot{\mathbf{u}}+\mathbf{C}\dot{\mathbf{u}}+\mathbf{f}(\mathbf{u}_o,\boldsymbol{\alpha}_o)+\mathbf{P}=\mathbf{F}$$

$$\mathbf{u}=\begin{bmatrix}\mathbf{u}_{ss}\\ \mathbf{u}_i\end{bmatrix},\quad \mathbf{M}=\begin{bmatrix}\mathbf{M}_{ss,ss} & \mathbf{0}\\ \mathbf{0} & \mathbf{M}_{i,i}^{ss}\end{bmatrix},\quad \mathbf{C}=\begin{bmatrix}\mathbf{C}_{ss,ss} & \mathbf{C}_{ss,i}\\ \mathbf{C}_{i,ss} & \mathbf{C}_{ii}^{ss}\end{bmatrix},\quad \mathbf{F}=\begin{bmatrix}\mathbf{F}_{ss}\\ \mathbf{F}_i\end{bmatrix}$$

$$\mathbf{f}(\mathbf{u})=\begin{bmatrix}\mathbf{f}_{ss}(\mathbf{u}_{ss},\mathbf{u}_i,\boldsymbol{\alpha}_{ss})\\ \mathbf{f}_i^{ss}(\mathbf{u}_{ss},\mathbf{u}_i,\boldsymbol{\alpha}_{ss})\end{bmatrix}+\begin{bmatrix}\mathbf{0}\\ \mathcal{F}^{-1}(\mathbf{S}_{reduced})*\mathbf{u}_i\end{bmatrix},\quad \mathbf{P}=\begin{bmatrix}\mathbf{0}\\ \mathcal{F}^{-1}(\mathbf{RF}\cdot2\pi\cdot\delta(\omega))\end{bmatrix}$$

$$\mathbf{RF}=-\mathbf{S}_{i,soil}\cdot\mathbf{S}_{soil,soil}^{-1}\cdot\mathbf{X}_{soil}(\mathbf{u}_o,\boldsymbol{\alpha}_o)+\mathbf{X}_i(\mathbf{u}_o,\boldsymbol{\alpha}_o)$$

$$\mathbf{S}_{reduced}=\mathbf{S}_{i,i}^{soil}(\mathbf{u}_o,\boldsymbol{\alpha}_o)-\mathbf{S}_{i,soil}(\mathbf{u}_o,\boldsymbol{\alpha}_o)\cdot\mathbf{S}_{soil,soil}^{-1}(\mathbf{u}_o,\boldsymbol{\alpha}_o)\cdot\mathbf{S}_{soil,i}(\mathbf{u}_o,\boldsymbol{\alpha}_o) \quad (10)$$

The extracted, reduced, complex matrices $\mathbf{RF}(\mathbf{u_o},\boldsymbol{\alpha_o})$ and $\mathbf{S}_{\text{reduced}}(\mathbf{u_o},\boldsymbol{\alpha_o})$ are capable of emulating the local dynamic behavior traits of the foundation-soil condensed segment in regard to small trajectories of the segment DOFs near the variable state $\mathbf{s_o}=[\mathbf{u_o}, \boldsymbol{\alpha_o}]^{\mathbf{T}}$.

2.1 Truncated states selection of condensed system

Due to the infinite number of different values of the soil-foundation segment variable states $\mathbf{s_o}=[\mathbf{u_o},\boldsymbol{\alpha_o}]^{\mathbf{T}}$, it is numerically impossible to retrieve the condensed complex matrix pairs **RF** and $\mathbf{S}_{\text{reduced}}$ for each possible displacement and plasticity variables combination of the soil foundation internal DOFs. As a result, a selection of representative variable states in connection to the behavior of the interface DOFs is essential.

An effective yet computationally non-burdening truncation on the possible variable state combinations can be accomplished using the static pattern of deformation of the condensed segment. The tangent stiffness matrices $\nabla_{\mathbf{u}_i}\mathbf{f}_i^{soil}, \nabla_{\mathbf{u}_{soil}}\mathbf{f}_i^{soil}, \nabla_{\mathbf{u}_i}\mathbf{f}_{soil}, \nabla_{\mathbf{u}_{soil}}\mathbf{f}_{soil}$ and residual force vectors $\mathbf{f}_i^{soil}, \mathbf{f}_{soil}$ corresponding to a specific interface DOF variable state are calculated from the condensed segment static equation system under the externally imposed displacement values of a combination of interface DOFs displacements $\mathbf{u}_{i,o}$. In more detail, the static version of the soil foundation segment illustrated in equation (11) can be solved for a known interface displacement combination $\mathbf{u}_{i,o}$, leading to the internal DOF variables $\mathbf{u}_{soil,o}$ and $\boldsymbol{\alpha}_{soil,o}$. R_o is the unknown force vector of the interface DOFs and $\mathbf{H_{soil}}$ is the internal variable evolution function of the soil segment DOFs. Subsequently, the remaining variables of the state $\mathbf{s_o}=[\mathbf{u}_{i,o}, \mathbf{u}_{soil,o}, \boldsymbol{\alpha}_{soil,o}]^{\mathbf{T}}$ are now known and the calculation of the **RF** and $\mathbf{S}_{\text{reduced}}$ pair corresponding to the $\mathbf{s_o}$ state is possible. The static pattern assumption is only approximating the inelastic force to displacement vector of the subsoil internal DOFs. The validity of the proposed simplification is further studied in the implementation examples presented in the following sections.

$$\begin{bmatrix} \mathbf{f}_i^{soil}(\mathbf{u}_{i,o},\mathbf{u}_{soil,o},\boldsymbol{\alpha}_{soil,o}) \\ \mathbf{f}_{soil}(\mathbf{u}_{i,o},\mathbf{u}_{soil,o},\boldsymbol{\alpha}_{soil,o}) \\ \mathbf{H}_{soil}(\mathbf{u}_{i,o},\mathbf{u}_{soil,o},\boldsymbol{\alpha}_{soil,o}) \end{bmatrix} = \begin{bmatrix} R_o \\ 0 \\ 0 \end{bmatrix} \tag{11}$$

Through the aforementioned assumption, an **RF** and $\mathbf{S}_{\text{reduced}}$ matrix pair can now be coupled with a specific interface DOF displacement combination $\mathbf{u}_{i,o}$. Further truncation is accomplished through the integration of repetitive (i.e., unloading and pre-yielding) or asymptotic behaviors (*e.g* asymptotically linear post-yielding behavior) of the dynamic properties of the soil-foundation segment along with a definition of an expected operating range of interface DOF displacements within which the dynamic system is expected to behave.

3. PROPOSED MODEL ASSEMBLY

Since the inelastic dynamic behavior of the condensed soil foundation segment can now be extracted in the form of a preselected number of (reduced) complex matrix pairs **RF** and $\mathbf{S}_{\text{reduced}}$, it is possible to develop a modified LP model assembly capable of emulating such behavior. The predefined Type 3 LP design, proposed by Saitoh [18], is selected as the basis of the newly developed inelastic LP model. The resulting LP model for the scenario of a single interface DOF is illustrated in Figure 2.

As shown, the LP model consists of one *inelastic base* component S_{base} capable of emulating the *quasi-static* properties of the condensed soil-foundation segment, while additional complementary components are accordingly calibrated to match the intensity-dependent dynamic traits of the soil-foundation system. The idea here is that the base component can be taken as a standard elastoplastic or hypoplastic macroelement according to the literature, depending on the specific foundation. In regard to the complementary components aiming to capture the dynamic behavior, conventional solutions are not capable of providing a sufficient accuracy. This is due to the fact that elastic equation terms of conventional components provide very limited capabilities of different impedance function emulation for different strain levels of the macrolement base component. To this end, inelastic components $s_{comp,i}$ are integrated in the LP model as presented in the following paragraphs. The component $s_{comp,i}$ is externally controlled, as its current stiffness is governed by the displacement and internal plastic variables of the macroelement base component and not the relative displacement of the respective nodes the component connects. On the other hand, components $c_{i,up}$, $c_{i,down}$ and m_i follow the conventional definition of dashpot and mass components respectively.

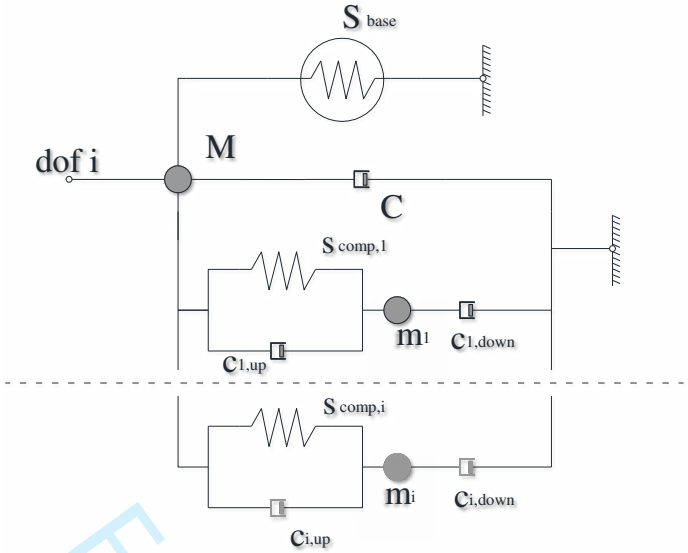

Figure 2. Physical representation of the proposed Lumped Parameter Model

3.1 Derivation of externally controlled inelastic components

The $s_{comp,i}$ components of the proposed LP assembly follow the multi-linear inelastic constitutive law illustrated in equation (12). The aforementioned components current stiffness is associated with the internal plasticity variables $\boldsymbol{\alpha}_{base}$ and interface DOF displacement u_{base} of the selected base component macroelement.

$$\dot{F}_{comp} = k_{comp}\left(\boldsymbol{\alpha}_{base}, u_{base}\right)\cdot \dot{u}_{comp}$$

$$where \quad k_{comp}\left(\boldsymbol{\alpha}_{base}, u_{base}\right) = \begin{cases} k_o & if\ [\boldsymbol{\alpha}_{base}, u_{base}]^{\mathrm{T}} < \mathbf{c}_o\ or\ \ Unloading \\ \vdots & \\ k_n & if\ \ \mathbf{c}_{n-1} < [\boldsymbol{\alpha}_{base}, u_{base}]^{\mathrm{T}} < \mathbf{c}_n \end{cases} \tag{12}$$

The variable Vector $\boldsymbol{\alpha}_{base}$ corresponds to the base component S_{base} internal variables at the current state of the system, $\mathbf{c}_i$ are constant value vectors controlling the regions for which $\boldsymbol{\alpha}_{base}$ and u_{base} correspond to different spring stiffness k_i, while u_{comp} is the relative displacement between the two nodes defining the component s_{comp}.

The selection of an externally controlled component lies within the nature of the extracted dynamic traits, as it provides with a different stiffness value and thus dynamic properties of the overall LP model for every different interface DOF combination u_{base}. As presented in the previous sections, each extracted pair of **RF** and $\mathbf{S}_{\text{reduced}}$ has been affiliated with a specific combination of interface DOF displacements. As a result, the calibration process can be significantly more efficient in comparison to the use of conventional multi-linear inelastic springs. The components are numerically implemented to the LP assembly through the explicit Runge-Kutta iterative method.

3.2 LP model Impedance Functions

Through the definition of the base and complementary components of the assembly, it is now possible to generate the matrix expression of the proposed LP model in regard to a single DOF interface, as illustrated in equation (13).

$$\mathbf{f}_{LP}(\mathbf{u}) = \begin{bmatrix} f_{base}(\mathbf{u}) + f_{comp,1}(\mathbf{u}) \cdots + f_{comp,N}(\mathbf{u}) \\ f_{comp,1}(\mathbf{u}) \\ \vdots \\ f_{comp,N}(\mathbf{u}) \end{bmatrix} \quad \mathbf{M}_{LP} = \begin{bmatrix} M & 0 & \dots & 0 \\ 0 & m_1 & & \vdots \\ \vdots & & \ddots & 0 \\ 0 & \dots & 0 & m_N \end{bmatrix}$$

$$\mathbf{C}_{LP} = \begin{bmatrix} C + c_{up,1} \dots + c_{up,N} & -c_{up,1} & \dots & -c_{up,N} \\ -c_{up,1} & c_{up,1} + c_{down,1} & & \vdots \\ \vdots & & \ddots & 0 \\ -c_{up,N} & \dots & 0 & c_{up,N} + c_{down,N} \end{bmatrix} \tag{13}$$

The variable vector **u** corresponds to the displacement of the LP model's DOFs, $\mathbf{M}_{LP}$ represents the mass matrix of the LP model, $\mathbf{C}_{LP}$ represents the damping matrix of the LP model, while $\mathbf{f}_{LP}$ denotes the nonlinear force to displacement relation vector.

In a similar manner to the previously presented linearization process of the soil-foundation segment, it is possible to derive a linearized model of the LP dynamic system around a preselected state $\mathbf{u_o}$=[$u_{base,o}$, $\mathbf{u}_{comp,o}$] through the Taylor expansion of the nonlinear restoring force vector $\mathbf{f}_{LP}$. Through the affiliation of the interface DOF displacement u_{base} to a variable state combination of the LP model through the static pattern of deformation, it is possible to extract the model's $\mathbf{S}_{LP}$ and $\mathbf{RF}_{LP}$ matrix pairs, representing the dynamic behavior of the LP model for the u_{base} state. The impedance and restoring force functions $S_{LP,o}$ and $RF_{LP,o}$ at a preselected variable state o are illustrated in equations (Eq. 14-15).

$$S_{LP,o}(\omega) = K(\boldsymbol{\alpha}_{base,o}, u_{base,o}) - M\cdot\omega^2 + C\cdot\omega i + \sum_{i=1}^{N_{core}} \left(\frac{(k_{comp,i}(\boldsymbol{\alpha}_{base,o}, u_{base,o}) + c_{up,i}\cdot\omega i)(-m_i\cdot\omega^2 + c_{down,i}\cdot\omega i)}{k_{comp,i}(\boldsymbol{\alpha}_{base,o}, u_{base,o}) + c_{up,i}\cdot\omega i - m_i\cdot\omega^2 + c_{down,i}\cdot\omega i} \right) \tag{14}$$

$$RF_{LP,o}(\omega) = X + \sum_{i=1}^{N_{core}} \left(\frac{(k_{comp,i}(\boldsymbol{\alpha}_{base,o}, u_{base,o}) + c_{up,i}\cdot\omega i)\cdot x_i}{k_{comp,i}(\boldsymbol{\alpha}_{base,o}, u_{base,o}) + c_{up,i}\cdot\omega i - m_i\cdot\omega^2 + c_{down,i}\cdot\omega i} \right)$$

$$\text{Where} \quad X = f_{base}(\mathbf{u}_o) - K(\boldsymbol{\alpha}_{base,o}, u_{base,o})\cdot u_{base,o} + \sum_{i=1} \left(f_{comp,i}(\mathbf{u}_o, \boldsymbol{\alpha}_{base,o}) - k_{comp,i}(\boldsymbol{\alpha}_{base,o}, u_{base,o})\cdot u_{i,o} \right)$$

$$x_i = f_{comp,i}(\mathbf{u}_o, \boldsymbol{\alpha}_{base,o}) - k_{comp,i}(\boldsymbol{\alpha}_{base,o}, u_{base,o})\cdot u_{base,o} + k_{comp,i}(\boldsymbol{\alpha}_{base,o}, u_{base,o})\cdot u_{i,o} \tag{15}$$

As the dynamic matrix pairs extracted from both the proposed LP model and the targeted soil foundation segment are paired with the same variable states of the interface DOF displacements, it is possible to calibrate the LP model in order to match the matrix pairs generated by the soil-foundation segment.

4. CALIBRATION PROCESS OF THE PROPOSED MODEL

4.1 Model order reduction through LP model calibration

The model order reduction approach selected for the current study is materialized through the derivation of a reduced model capable of approximating the behavior of the targeted complex system. It is possible to formulate the model order reduction approach as an optimization problem illustrated in equation (16).

$$\begin{aligned} &\min_{S_r} f(M, M_r) \\ &\textit{subject to } g(M, M_r) \le 0 \\ &h(M, M_r) = 0 \end{aligned} \tag{16}$$

The variable M represents the targeting dynamic system ODE formulation, M_r is the reduced order system possessing a lower number of state variables in comparison to M and function f specifies the behavioral divergence between the targeted and reduced system. The functions g and h are inequality and equality constraints of the optimization problem, imposing attractor behavior and maintaining specific structure properties of the system M.

The optimization problem of eq. (16) can be reformulated on the specific scenario of the SSI system order reduction, through the appropriate derivations of the previously presented objective function and imposed constraint terms. In that case, the soil-foundation segment of the overall system is significantly condensed through the use of the inelastic LP model presented in the previous section as an adequate replacement. The order reduction problem takes the following multi-objective optimization form as illustrated in equations (eq. 17-18).

$$\min_{\mathbf{x}} \left(f_1(x),...f_n(x)\right) \quad subject\ to\ \mathbf{x} \geq 0 \tag{17}$$

$$\begin{aligned} f_o(\mathbf{x}) = &\sum_{i=1}^{m}\left[\mathrm{Re}\left(S_{Tar,o}(\omega_i)\right)-\mathrm{Re}\left(S_{LP,o}(\omega_i,\mathbf{x})\right)\right]^2+\sum_{i=1}^{m}\left[\mathrm{Im}\left(S_{Tar,o}(\omega_i)\right)-\mathrm{Im}\left(S_{LP,o}(\omega_i,\mathbf{x})\right)\right]^2 \\ &+\sum_{i=1}^{m}\left[\mathrm{Re}\left(RF_{Tar,o}(\omega_i)\right)-\mathrm{Re}\left(RF_{LP,o}(\omega_i,\mathbf{x})\right)\right]^2+\sum_{i=1}^{m}\left[\mathrm{Im}\left(RF_{Tar,o}(\omega_i)\right)-\mathrm{Im}\left(RF_{LP,o}(\omega_i,\mathbf{x})\right)\right]^2 \end{aligned} \tag{18}$$

where, index o denotes a specific interface DOF variable state ranging from 1 to n, $S_{\mathrm{Tar,o}}$ and $S_{\mathrm{LP,o}}$ indicate the impedance functions of the targeted and reduced LP system, respectively, on a given variable state o, while RF_{Tar} and RF_{LP} indicate the restoring force complex functions of the targeted and reduced LP system, respectively, on a given variables state o. Each objective function f_o follows a sum of least squares representation between the impedance and restoring force functions. Finally m corresponds to the number of measured frequency points of the targeted behavior.

4.2 Proposed algorithmic approach for the optimization process

The scalarization of the multi-objective optimization problem illustrated in equation (eq. 17-18) is selected as the most effective approach, as the problem's high number of objective functions can lead to computationally burdening solutions when a posteriori methods are introduced. The weighted-sum method, initially proposed by Zadeh [19], is a traditional popular method following an a priori preference on the selection of a Pareto optimal through appropriate importance related weighting of the objective functions. The initial optimization problem takes the following single objective form as illustrated in equation (eq. 19).

$$\min_{\mathbf{x}} g(\mathbf{x}) = \sum_{o=1}^{n} w_o \cdot f_o(\mathbf{x}) \quad subject\ to\ \mathbf{x} \geq 0 \tag{19}$$

As the objective function commonly behaves in a nonlinear, non-convex manner, an arbitrary implementation of a deterministic optimization approach can lead to local minima without expanding the LP model's potential to its full capacity. As a result, the algorithm used for the solution of the optimization problem of Eq. (19) consists of the combined efforts of a deterministic search method operating in a local level and a general plan operating in a global level. The local search method most efficiently suited for eq. (19) is the interior point trust region approach proposed by Coleman and Li [20]. According to this approach, the quadratic trust region sub-problem is approximately solved as the minimization of a quadratic problem subjected to an appropriate ellipsoidal constraint. The global level general plan is achieved through the multiple execution of the interior point trust region method, initiated from different stochastically generated locations $\mathbf{x_i}$ inside a prediction region (Fig. 2).

The termination criteria for the proposed optimization scheme consists of an iterative evaluation of the objective function value for the normalized static stiffness of the LP model, along with a maximum boundary on the number of the overall sampling points $\mathbf{x_i}$.

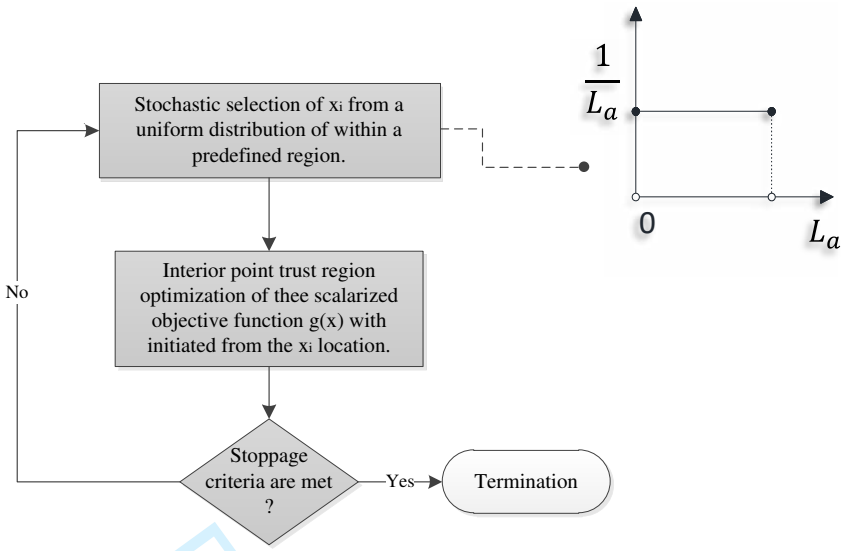

Figure 2. Multi-start algorithm used for the calibration process

5. METHOD VERIFICATION ON A SINGLE DOF INTERFACE SYSTEM

As presented in the previous paragraphs, the proposed procedure can provide a computationally viable alternative to the direct FEM approach for the solution of the SSI problem. However, the procedure is founded on a number of assumptions, which can render its efficiency questionable. To this end, it is essential to verify the proposed procedure through case specific examples where the procedure's efficiency can be tested under different conditions. The verification of the proposed procedure is accomplished through the case study of a single interface DOF representation of a strip foundation on homogenous clay soil as illustrated in Figure 3. In addition to the proposed inelastic LP model approach (M1), a simplified case of the presented LP assembly with conventional *elastic* complementary components, solely tuned to the elastic impedance function of the condensed segment (M2) is also implemented for reasons of efficiency comparison.

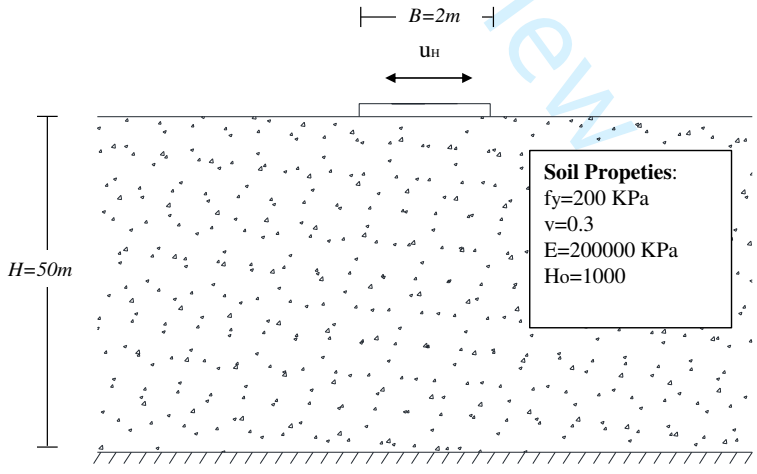

Figure 3.: Shallow foundation over uniform soil profile example (plane strain conditions)

As a targeted behavior is essential to the case study, a finite element model of the soil foundation segment has been constructed. The soil foundation system is simulated as a plane strain model of a rigid strip foundation over a uniform clay profile. The strip foundation is considered to be in full contact with the supporting soil domain. An elastoplastic constitutive law is implemented for the representation of the soil according to an

associative plasticity flow with isotropic hardening and a Von-Mises yielding criterion. The soil constitutive law properties are summarized in Table I. The overall FEM model includes a 100m x 50m truncated region of the semi-infinite soil domain, where absorbing boundaries are introduced at the side of the model according to [21], and a rigid bedrock is assumed at a depth of 50m.

Table I . Properties of the selected soil materials

Yielding Criterion	E(KPa)	Hardening Param. H_o	Poisson's Ratio ν	Yield Stress in Pure shear f_y (KPa)
Von Mises	200000	1000	0.3	200

5.1 LP models calibration process

For the current study and for simplicity purposes, only one DOF is considered at the interface between the soil foundation segment and the superstructure, i.e., corresponding to the horizontal displacement of the centroid of the strip foundation. As a result, a single DOF elastoplastic constitutive law is utilized as the base component of the LP model of both the complete method (M1) and the conventional complementary component method (M2). The selected constitutive law is described by the following elastoplasticity loading/unloading conditions (eq.20) and yielding equation (eq.21).

$$\dot{\gamma} \geq 0 \,,\, \Phi(F) \leq 0 \,,\, \dot{\gamma} \cdot \Phi(F) = 0 \tag{20}$$

$$\Phi(F) = \left| F - H(e_p) \right| - G(a) \tag{21}$$

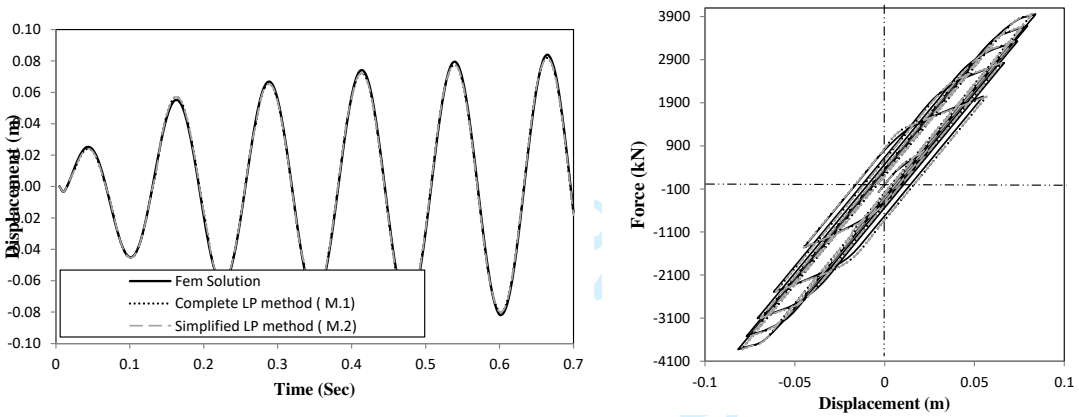

Figure 4.: Efficiency of the simplified and complete LP models under quasi-static excitation (a) displacement to pseudo-time, and (b) force to displacement relation

where *F* denotes the generalized force of the base component and *Φ* is the yielding criterion of the elastoplastic constitutive law. With regard to the terms of the yielding function, *H* corresponds to the kinematic hardening function, *G* to the isotropic hardening function and e_p and *a* are the isotropic and kinematic hardening parameters. A polynomial form is selected for the representation of the hardening function *G* and *H*, where the polynomial factors are calibrated according to the quasi-static behavior of the FEM model. Results of the base component efficiency for quasi-static loading are illustrated in Figure 4.

For this single interface DOF the system's dynamic traits are extracted from the FEM model for four different variable state combinations in accordance to preselected displacements of the interface DOF ($u_{1,o}$=0mm, $u_{2,o}$=10mm $u_{3,o}$=16mm $u_{4,o}$=29mm, , $u_{5,o}$=66mm, $u_{6,o}$=100mm). As observed, an isotropic hardening mechanism is mainly controlling the cyclic behavior of the targeted system while a linear force-displacement behavior is asymptotically dominating the plastic strain region of the system. Through the exploitation of the aforementioned observations the four variable states corresponding to $u_{1,o}$ - $u_{4,o}$ interface DOF displacements are sufficient data for the representation of the system's IF and RF matrix pairs at any other given state as illustrated in Figure 5. Due to the observed isotropic loading surface evolution of the FEM model, the extracted states are matched to the isotropic internal plastic threshold values of the statically tuned macroelement through the calculation of the plastic threshold values for the given variable state displacement.

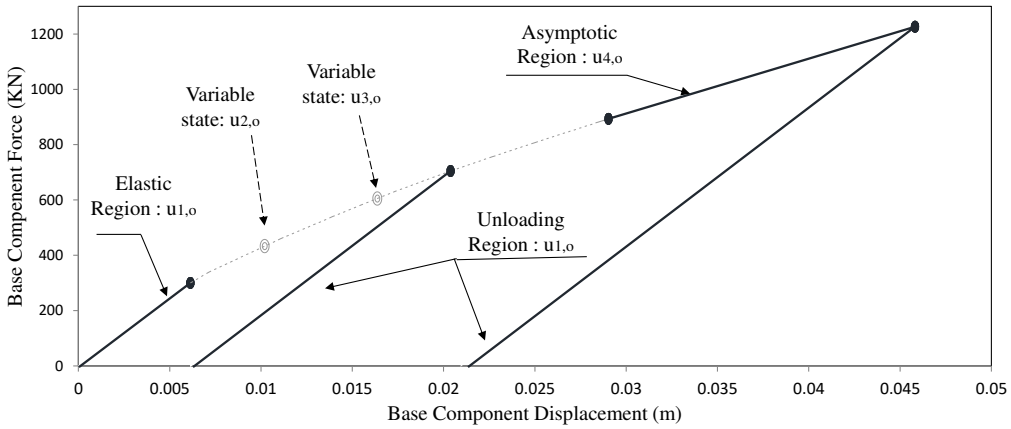

Figure 5. Variable states truncation through exploitation of repetitive and asymptotic behavior

The condensed segment's impedance function and restoring force matrix pairs $S_{reduced}$ and RF are extracted through the appropriate linearization and dynamic condensation of the system in the frequency domain in regard to the preselected interface DOF. The extracted properties are used as a target for the calibration of the complementary components of the complete method (M.1), while the simplified method (M.2) is tuned according to the elastic impedance function of the targeted system. Both LP models are utilized with a number of 4 cores. The calibration results are illustrated in Figures 6 and 7 for the interface displacement states $u_{1,o}$ to $u_{6,o}$.

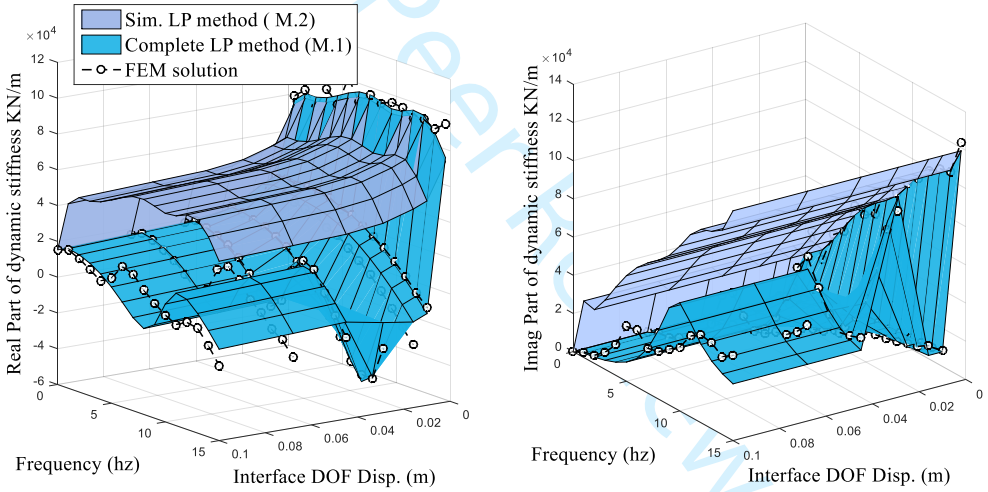

Figure 6. Calibration efficiency of the lumped parameter models for the Impedance Functions

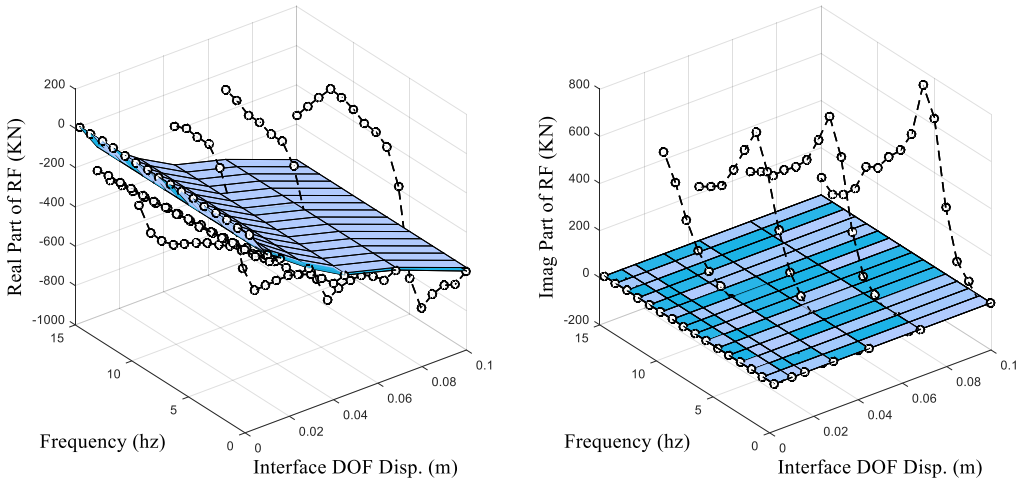

Figure 7. Calibration efficiency of the lumped parameter models for the RF functions

As observed in Figure 6 the dynamic stiffness functions of the targeted dynamic system is accurately captured by the complete LP method (M.1), while the simplified method (M.2) overestimates the dynamic stiffness values for almost all the frequency range of 0 to 15 Hz. The restoring force functions RF illustrated in Figure 7 presents some limitations on the emulating capabilities of the RF complex matrix by both methods (M.1 and M.2). These limitations are imposed by the static pattern based truncation of the selected variable states presented in the previous paragraphs. The formulation of the proposed LP assembly leads to zero internal displacements on the internal components S_{comp} for an imposed displacement at the interface DOF of S_{base}, thus nullifying the S_{comp} governed terms in xi of equation (eq.15). The aforementioned limitations could possibly be eradicated through the use of a modal based generated truncation pattern however such an approach is beyond the scope of the current study.

5.2 Time domain verification of the proposed model

The time domain verification of the proposed method is an essential step to assess the efficiency of the proposed model. As a result, a time history case study is presented in the following paragraphs. The dynamic response of the soil-foundation interface DOF under harmonic excitations on a frequency range of 0.5-4Hz (a typical range for earthquake engineering applications) is compared between the two LP model reduction methods and the FEM model. The harmonic excitations are directly applied on the interface DOF of the targeted system without the presence and influence of a superstructure, as the existence of the latter could mask the response of the SSI system. Two different amplitude levels of the excitations are included in the case study A_1=*200KN* and A_2=*1500KN*. For the case of the low intensity level the targeted system behavior is limited within the elastic domain (Figures 8-9). On the other hand, for the scenario of the higher intensity, the system significantly surpasses its yielding point (Figures 10-11).

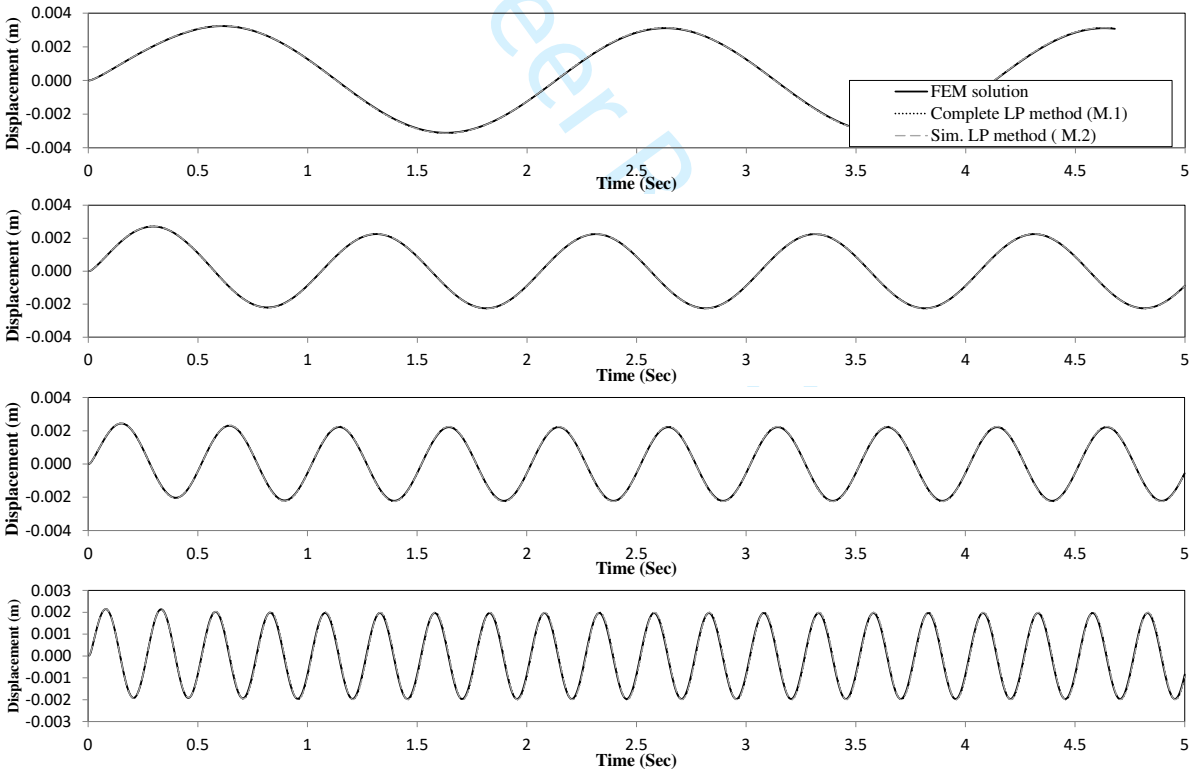

Figure 8. Low intensity dynamic response of LP models, displacement to time relationship

As observed in Figures (Figures 8-9) depicting the low intensity / elastic SSI response case, both the complete method (M.1) and the simplified approach (M.2) emulate the elastic dynamic behavior of the targeted FEM model in an accurate manner. This is anticipated since both models target the elastic dynamic properties during the calibration process.

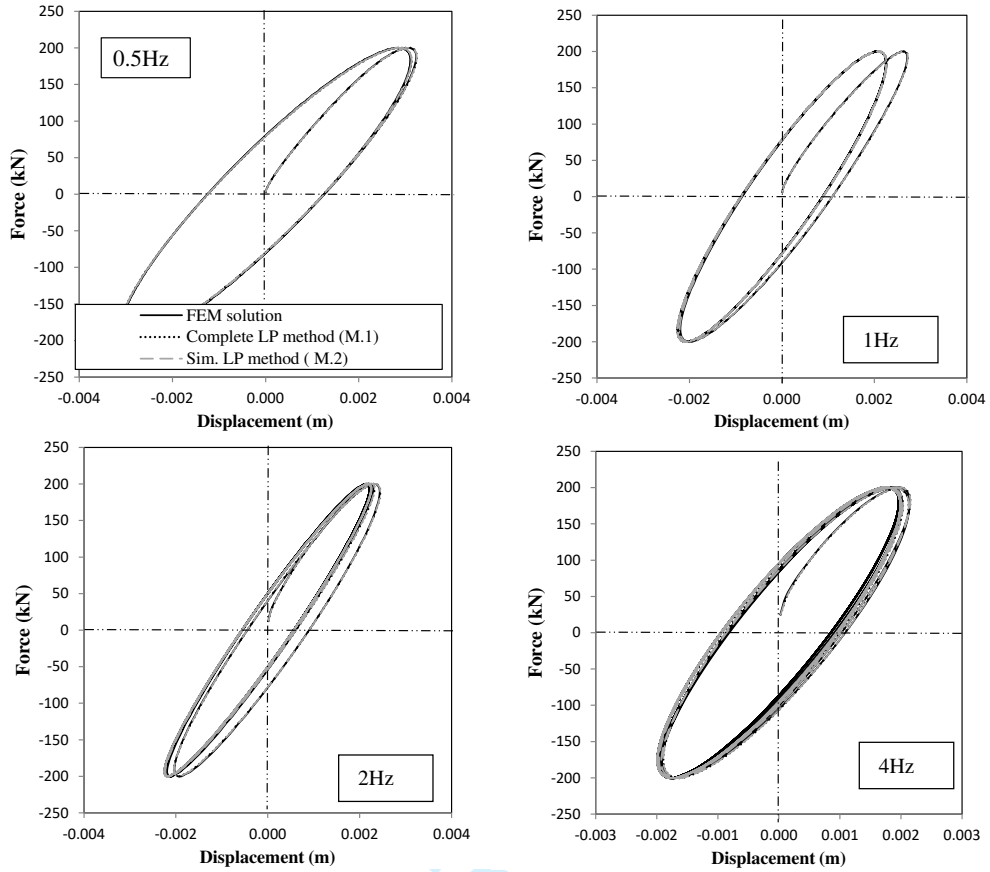

Figure 9. Low intensity dynamic response of LP models, Force to displacement relationship

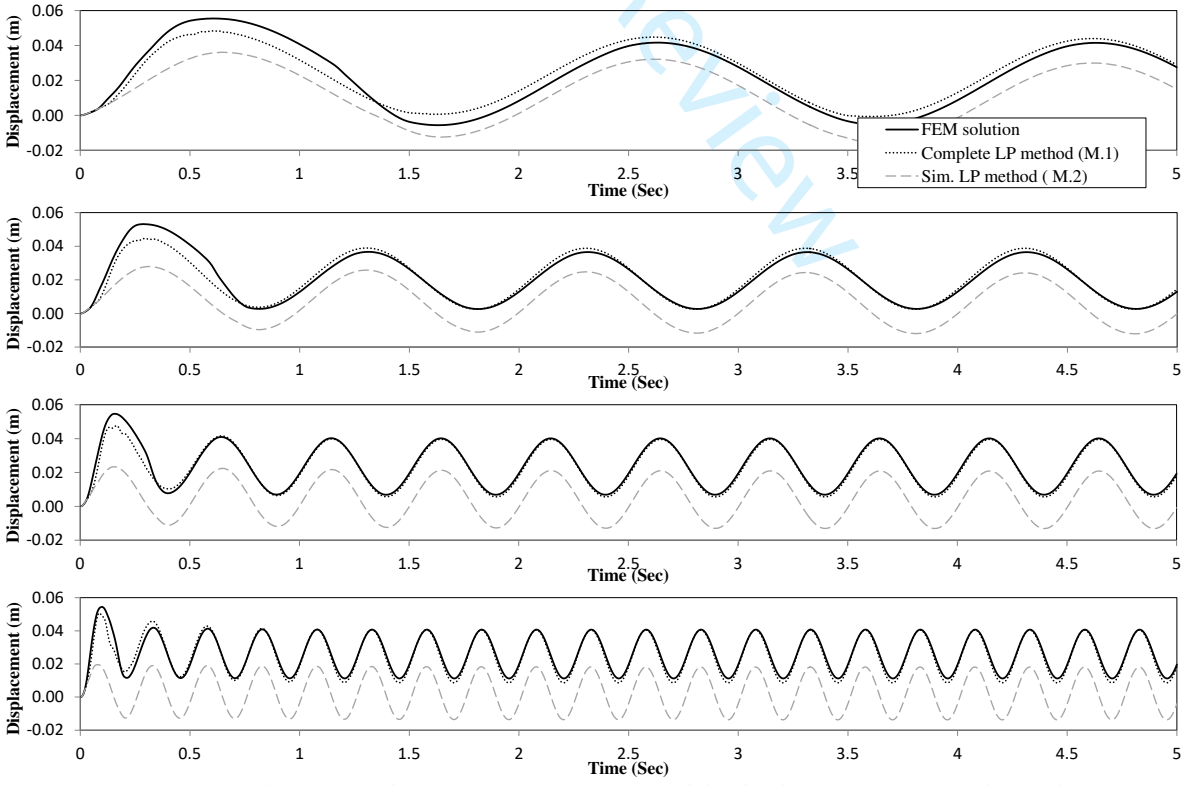

Figure 10. High intensity dynamic response of LP models, displacement to time relationship

For the higher excitation intensity scenario, the subsoil region demonstrates permanent plastic deformation as illustrated in Figures (Figures 10-11). It is observed that within the selected frequency range 0.5-4Hz, the post yield behavior of the simplified LP approach (M.2) is less efficient in comparison to the proposed method (M.1). This can be attributed to the fact that method M.2 exhibits a limited tuning process of the conventional complementary components and naturally, it cannot maintain a behavioural accuracy in intensity or frequency regions excluded from the calibration process. Additionally, as expected, the observed error is higher for higher frequencies where the static components of the reduced methods are less dominant.

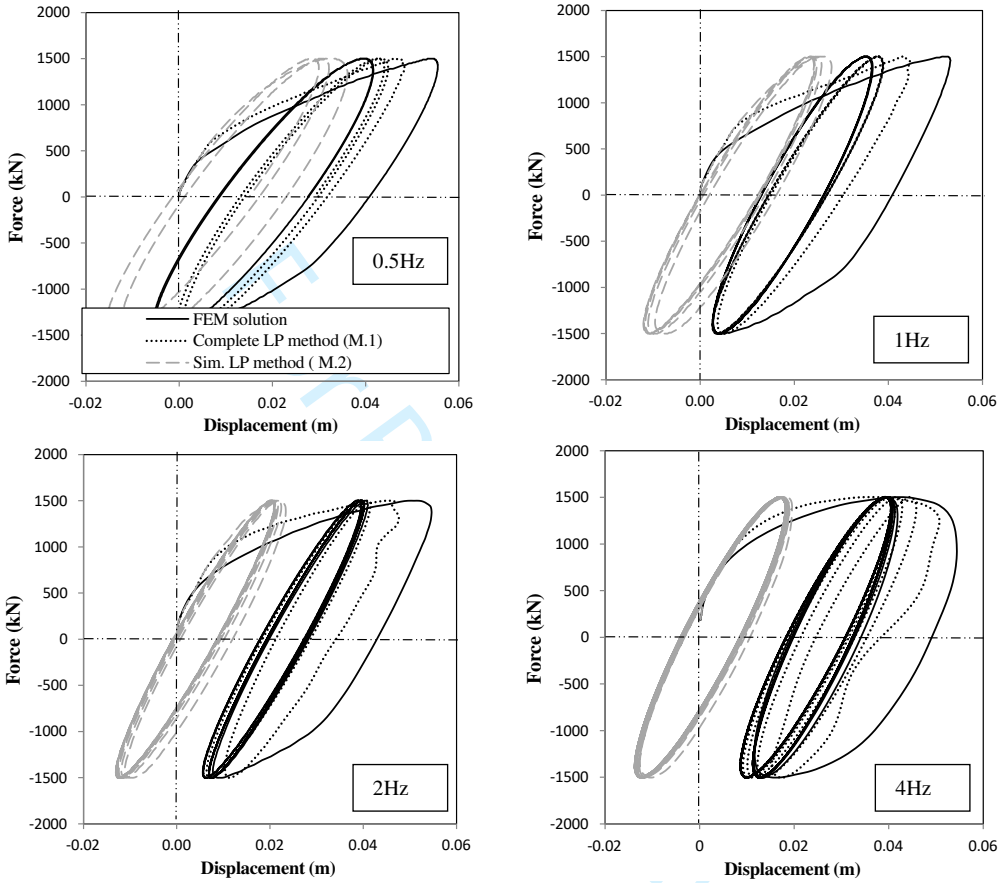

Figure 11. High intensity dynamic response of LP models, Force-displacement relationship

A second comparison is performed in Fig. 11 on the basis of a force-displacement relationship. It is evident that the complete proposed approach is superior to the simplified one and is able to match very closely the target FEM response. Additionally it can be observed that the yielding state displacement of the FEM system is lower in comparison to the one used in the base component of the complete (M.1) and simplified (M.2) LP method. This observation can lead to the conclusion that inelastic properties of the system are rate dependent, and subsequently the use of a rate independent statically calibrated macroelement can lead to a decrease in accuracy under specific circumstances.

6. METHOD VERIFICATION ON A MULTIPLE DOF INTERFACE SYSTEM

Through the verification process presented in the previous section, the efficiency of the proposed method and its simplified version has been determined for a single DOF interface system. However the aforementioned case study is mainly concentrated on the determination of the proposed method's efficiency under extreme conditions and the amplitudes A_1=*200KN* and A_2=*1500KN* of the harmonic excitations used for the low and high intensity cases of the study are the lower and higher extremes of a possible lateral loading applied on the foundation in question. In order to portray the behaviour of the proposed method in a more probable loading scenario, a case study of a bridge pier SSI problem under both harmonic and earthquake excitations is studied in the follow-

ing paragraphs. For this case study the three DOFs (u_x,u_z and θ_y) at the base of the foundation are selected as the interface region of the reduced soil foundation system.

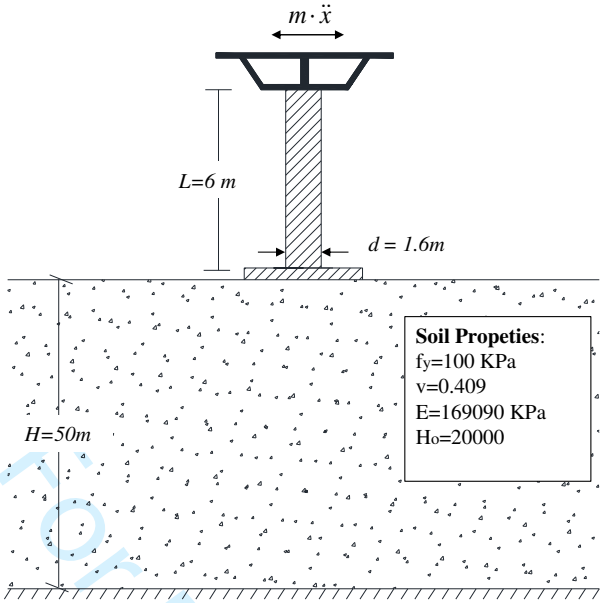

Figure 12. Bridge Pier SSI plane strain problem

As a targeted behavior is essential to the case study, a finite element model of the soil foundation segment has been constructed in a similar manner to the previous paragraph. The soil-foundation system is simulated as a plane strain model with a rigid element shallow foundation of 1m width at the out-of-plane direction. The foundation is considered to be in full contact with the supporting soil domain. An elastoplastic constitutive law is implemented for the representation of the soil according to an associative plasticity flow with isotropic hardening and Von-Mises as the law's yielding criterion. The soil constitutive law properties are summarized in Table III. As previously, the overall FEM model includes a 100m x 50m truncated region of the semi-infinite soil domain, where absorbing boundaries are introduced at the side of the model according to [21], while a rigid bedrock is simulated at the 50m depth of the model. The pier superstructure is simulated as a beam element directly connected to the foundation interface DOFs, with properties presented in Table II. A gravity load combination of a vertical force equal to 800 KN is applied on the top of the superstructure.

Table II. Multiple interface DOF case study: Superstructure Properties

Pier Height h(m)	Young Modulus E(MPa)	Mass M (tn)	Pier Diameter d(m)	Moment of Inertia I (m^4)
6	29000	350	1.4	0.188574

Units are considered per unit length of the strip footing

Table III. Multiple interface DOF case study: Soil Domain Properties

Yield Stress in Pure shear f_y (Kpa)	Young Modulus E(Kpa)	Poisson ratio V	Linear Isotropic hardening factor Ho
100	169090.9	0.409	20000

6.1 LP model calibration

The calibration process of the proposed LP model is initiated through the selection of an appropriate base component. The base component macroelement selected for the specific case study is an elastoplastic constitutive law with associative elliptical yielding function and mixed hardening, as depicted in equations (Eq. 22-24).

$$\dot{\mathbf{F}} = \mathbf{D}(\mathbf{F}, \boldsymbol{\alpha}) \cdot \dot{\mathbf{u}} \tag{22}$$

$$\mathbf{D} = \mathbf{D}_{el} - \mathrm{H}(\dot{\gamma}) \cdot \frac{\mathbf{D}_{el} \cdot \frac{\partial \Phi}{\partial \mathbf{F}} \cdot \frac{\partial \Phi}{\partial \mathbf{F}}^{T} \cdot \mathbf{D}_{el}}{\frac{\partial \Phi}{\partial \mathbf{F}} \cdot D_{el} \cdot \frac{\partial \Phi}{\partial \mathbf{F}} + \frac{\partial \Phi}{\partial \mathbf{F}} \cdot \mathbf{L}_{kin} \cdot \frac{\partial \Phi}{\partial \mathbf{F}}^{T} + L_{iso}} \tag{23}$$

$$\Phi(\mathbf{F}) = \left(\frac{H - a_{k,H}}{H_O} \right)^2 + \left(\frac{M - a_{k,M}}{M_O} \right)^2 + \left(\frac{V - a_{k,V}}{V_O} \right)^2 - \mathrm{c}_{\mathrm{y,o}} + L_{iso} \cdot a_{iso} \tag{24}$$

The variable $\mathbf{D}_{el}$ corresponds to the elastic stiffness matrix of the macroelement, $\mathbf{u}$ is the displacement vector of the interface DOFs , $\mathbf{F}$=[V, H , M] is the force vector of the interface DOFs, Φ is the elastoplastic macroelement yielding criterion, $a_{k,i}$ are the kinematic hardening internal parameters and a_{iso} is the isotropic hardening internal parameter. The constant parameters H_o,M_o,V_o , L_{iso} and $c_{y,o}$ along with the diagonal $\mathbf{L}_{kin}$ matrix are all calibrated through a least square optimization process in order to achieve a successful matching with the quasi-static behaviour of the targeted system. The efficiency of the calibrated macroelement is illustrated in Figure 13 for the vertical DOF under isolated vertical loading and in Figure 14 for the rotational and horizontal displacement DOFs under a vertical load F_o=800KN. The rate of the applied moment is equal to My=Fx*h .

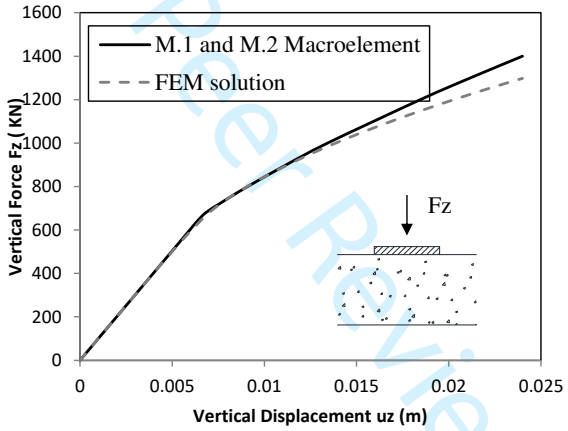

Figure 13. Vertical Force to vertical displacement relation of the LP and FEM models under monotonic static loading

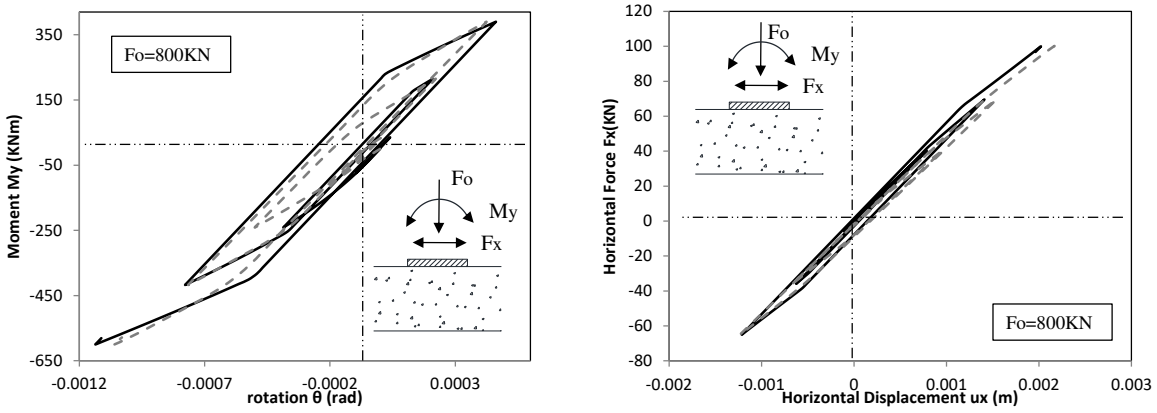

Figure 14. a) Moment to rotation and b) Force to displacement relation of the LP and FEM models under quasi static loading for the gravity load F_o=800KN

As the base component of the macroelement has now been generated it is possible to continue with the calibration of the complementary components of the M.1 and M.2 LP models. For the M.2 LP model the elastic impedance function is sufficient. For the M.1 method an initial truncation of the state variable combinations of the soil foundation segment is accomplished through the assumption of the static pattern of deformation. Additionally small alterations of the initial settlement of the foundation induced by the gravity force of the deck F_z=800 KN are expected. Further elimination of the selected state variables is accomplished through the definition of the elastic and operational regions of the horizontal and rotational interface DOFs. As a result, nine different interface DOF variable states are selected as illustrated in Table IV within the operational range of horizontal displacement -3 to 3 mm and rotation -0.3 to 0.3 mrad. A broader variable states range, up to the asymptotic high strain behavior of the foundation-soil system is a more appropriate approach if an estimation of the system's operational range is not available, as presented in the previous case study.

The expected error generated from the static pattern assumption is calculated for the loading scenario of the bridge gravity load combined with a harmonic horizontal excitation on the foundation level. The mean absolute percentage error (MAPE) of the subsoil DOF displacements for the moment of peak horizontal excitation with frequency f_o=4Hz is illustrated in figure 15. The maximum MAPE generated on the tangent stiffness matrix terms of each element for the same loading scenario is illustrated in figure 16a. The maximum MAPE of the element stiffness matrix terms for harmonic excitations with different frequencies is illustrate in 16b.

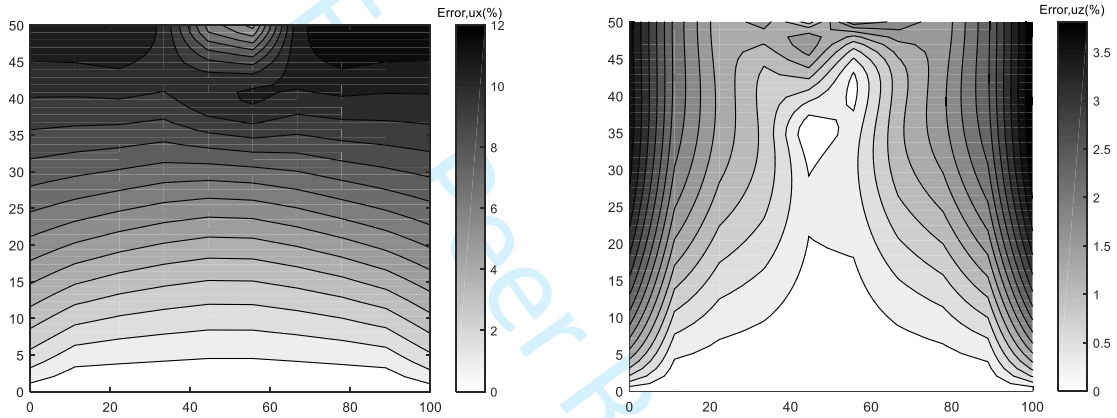

Figure 15. MAPE of subsoil DOFs variable state under the static pattern assumption for the a)horizontal u_x b)and vertical u_y displacements

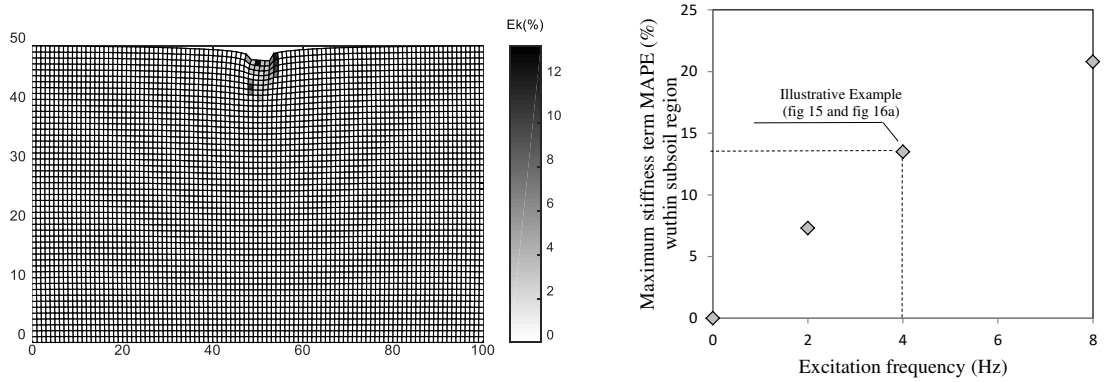

Figure 16. a) Distribution of tangent stiffness MAPE produced under the static pattern assumption b) Maximum tangent stiffness MAPE for harmonic excitations with different frequency

According to the illustrated results of figure 15, the displacement state divergence is observed to be higher on the left and right boundaries of the soil domain and identical on the fixed bottom boundary. Such an error concentration is expected as the Lysmer boundary conditions utilized on the specific case study provide with no reaction for the scenario where the static pattern assumption is implemented. However as illustrated in figure 16a, the error observed in regions far from the foundation has negligible influence on the calculation of the system's Impedance functions as little to no difference is observed on the tangent stiffness and internal plasticity variables of the subsoil elements within these regions. On the other hand for the near field region, the error is zero on the interface Dofs of the foundation and low for the region underneath the foundation. The displace-

ment error at the interface DOFs is by definition zero as the targeted displacement values are imposed at interface DOFs during the static pattern assumption. For the remaining DOFs on the near field region, static assumption is observed to be closely approximating the displacement distribution for a realistic excitation frequency. The maximum error generated on the tangent stiffness terms among all the subsoil elements for different excitation frequencies is illustrated in figure 16b.

Table IV. Selected Variable States

	vs.1	vs.2	vs.3	vs.4	vs.5	vs.6	vs.7	vs.8	vs.9
Fx (KN/m)	0	0	0	±40	±40	±40	±120	±120	±120
Fz(KN/m)	0	-800	-800	-800	-800	-800	-800	-800	-800
My(KNm/m)	0	±150	±350	0	±150	±350	0	±150	±350

For each selected variable state of the soil foundation segment, a 3x3 impedance function matrix and RF matrix are generated through the proposed procedure described in section 2. The impedance function and RF matrix pairs are directly calculated through the extraction of the tangent stiffness $\nabla \mathbf{f}$, mass M and damping C matrices of the FEM model and further calculations are performed in the frequency domain as illustrated in equation (eq.10). As the proposed approach has low emulating capabilities for the RF matrix, the optimization process is concentrated on capturing the impedance function matrices behavior. The non-diagonal coupling terms of each impedance function matrix are of negligible significance, thus are not taken into account in the current case study. The impedance function results of the calibration of the proposed LP method for the elastic variable state vs.1 and the variable state region of vs.2-vs.9 are illustrated in Figures 17-19. Both M.1 and M.2 LP models are utilized with a number of 4 cores for each interface DOF.

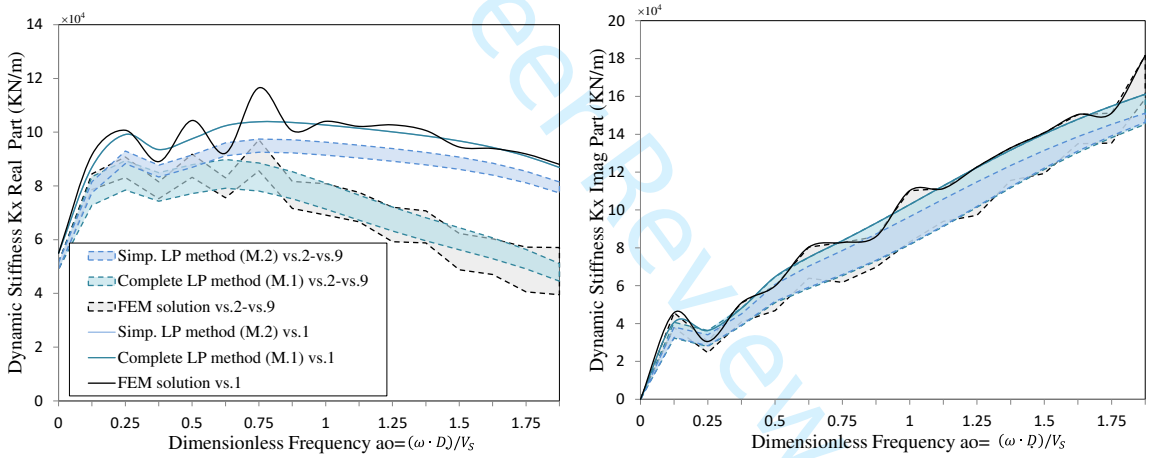

Figure 17. a) Real Part and b) Imaginary part of Kx impedance functions for the selected variable states

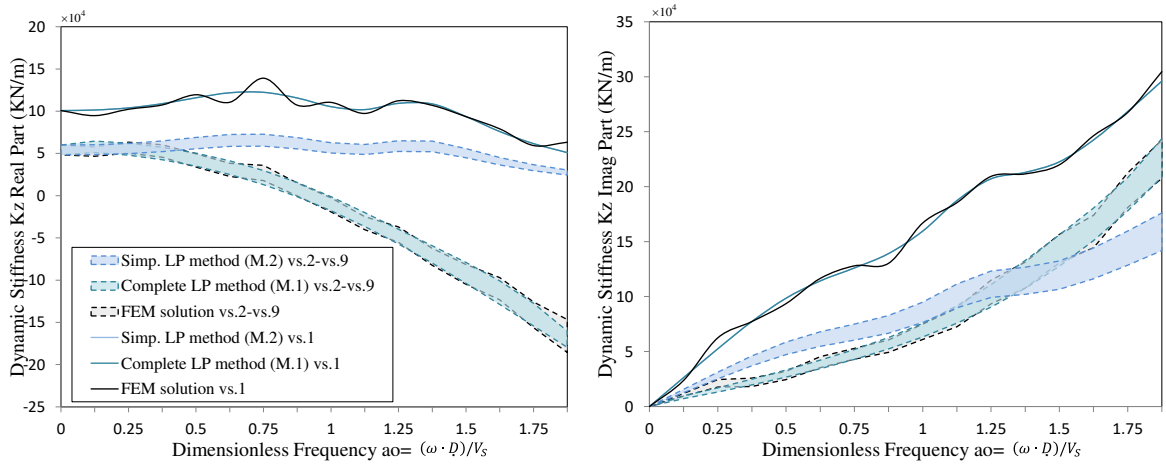

Figure 18. a) Real Part and b) Imaginary part of K_z impedance functions for the selected variable states

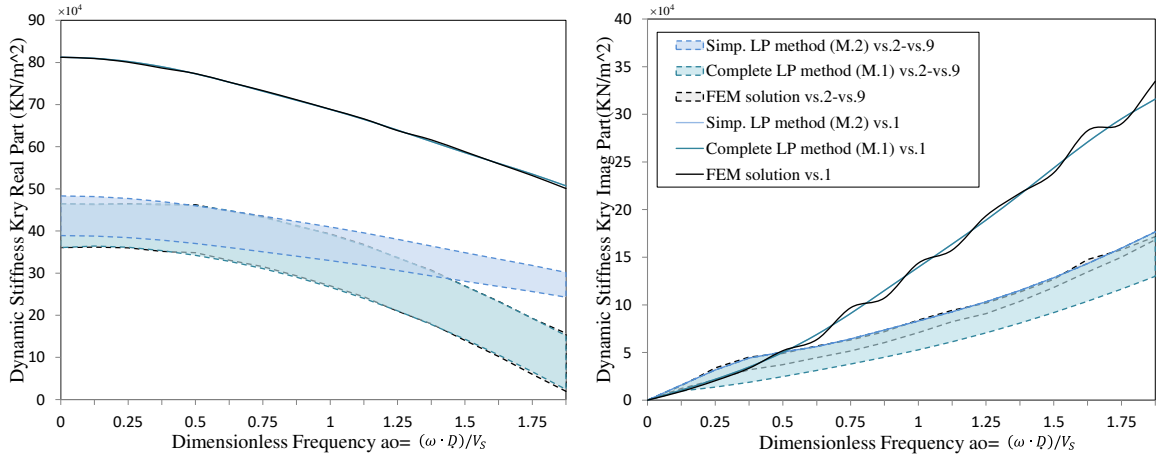

Figure 19. a) Real Part and b) Imaginary part of K_{ry} impedance functions for the selected variable states

As observed in the aforementioned figures, for the elastic variable state vs.1 both M.1 and M.2 LP methods are efficiently emulating the targeted FEM behavior for the three interface DOF impedance functions K_x,K_z and K_{ry}. For the remaining variable states located in the plastic strain region, it can be observed that the impedance functions generated by the M.1 LP model are accurately representing the extracted FEM impedance functions. On the other hand the M.2 model impedance functions tend to diverge from the targeted FEM impedance functions for frequencies higher of 5 Hz on all three interface DOFs.

6.2 Time domain analysis under harmonic excitations

The efficiency of the complete (M.1) and simplified (M.2) LP methods in the time domain is initially measured through the time history analysis of the case study example under a selection of harmonic excitations in the frequency range 1-4Hz. The harmonic excitation with acceleration amplitude $a_o=0.3g$ is directly assigned on the head of the pier superstructure in the form of a horizontal inertial force, amplified by the superstructure mass. The results of the displacement of the foundation are illustrated in Figures 20-21 for the following different approaches of the target FEM model, the M.2 simplified LP method, the M.1 complete LP method and for reasons of comparison a sole static macroelement.

As observed in the results depicted in Figures 18a and 18b, in the scenario of lower frequency excitations (f_e=1Hz and 2Hz), both LP methods M.1 and M.2 are capable of efficiently emulating the dynamic behavior of the targeted system. The behavior of M.1 and M.2 LP methods are observed to be almost identical for the lower frequency range as the inelastic impedance functions portray small differences in comparison to the elastic impedance functions of the condensed system. In the scenario of a higher frequency excitation (f_e=8Hz) the M.1 LP method is capable of providing a dynamic response with higher matching accuracy in comparison to the M.2 simplified LP method as illustrated in Figure 18c. Additionally, the static approach of the sole macroelement representation is depicted to match efficiently the rotational behavior of the condensed system for lower frequency scenarios, while a higher error is depicted in comparison to both M.1 and M.2 LP methods on any other response scenario.

Following the aforementioned observations, it is clear that the efficiency of any of the order reduction methods integrated in the current case study is highly correlated to the nature of the extracted dynamic properties of the targeted system. More specifically, the static macroelement approach can emulate the behavior of a targeted dynamic system with an acceptable accuracy only under the scenario of targeted impedance functions with close to constant real part behavior and an imaginary part of negligible amplitude. The simplified approach M.2 can lead to an acceptable accuracy as long as a high resemblance is portrayed between the different variable state impedance functions extracted from the targeted dynamic system.

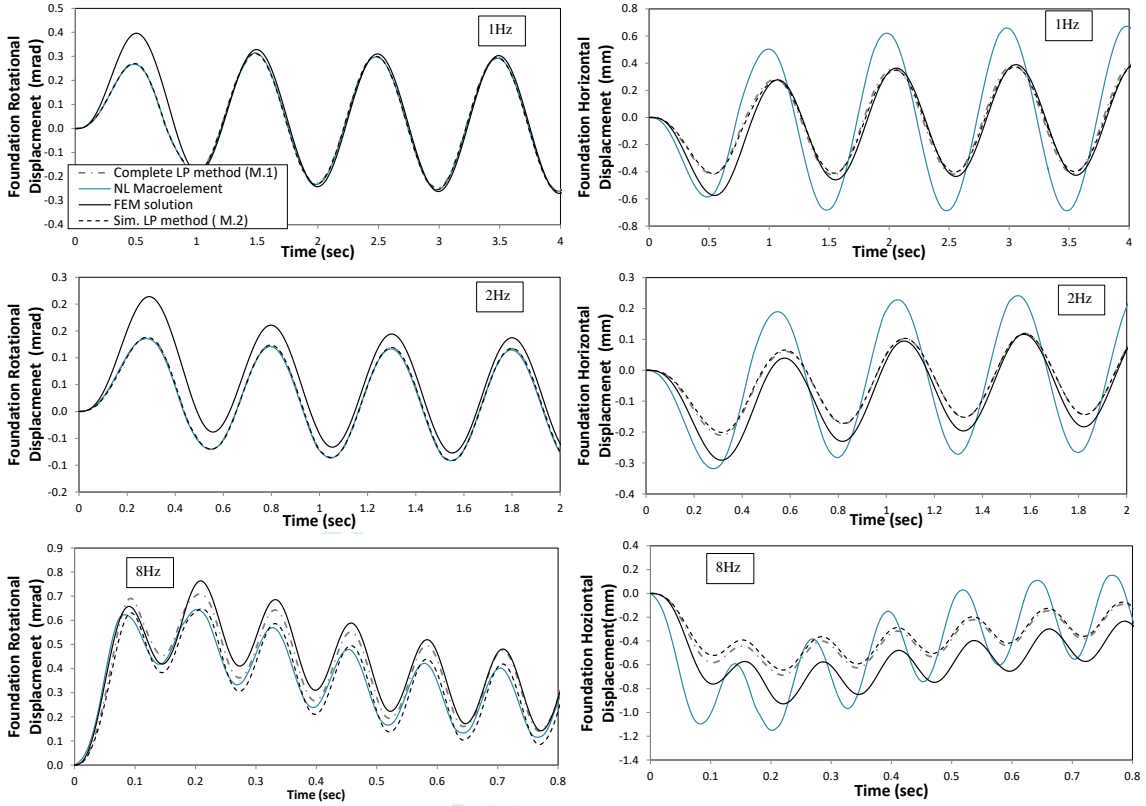

Figure 20. Foundation rotational and horizontal displacement response for the a) 1Hz b) 2Hz and c) 8Hz harmonic excitation

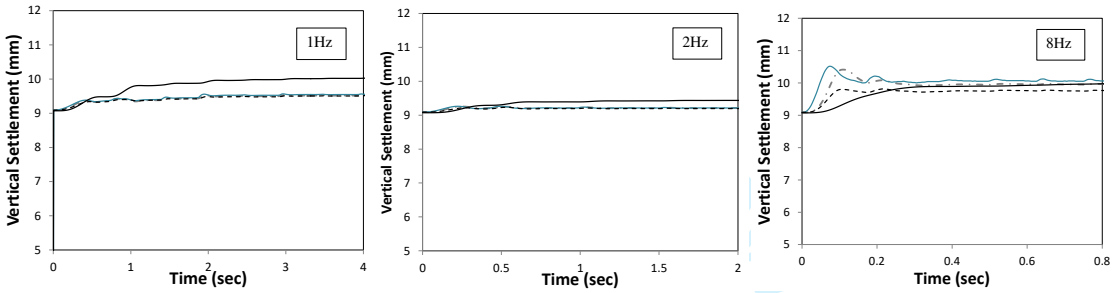

Figure 21. Foundation settlement for the a) 1Hz b) 2Hz and c) 8Hz harmonic excitation

6.3 Time domain analysis under earthquake excitation

As a final step, the proposed methods M.1 and M.2 along with the targeted FEM model and the static macroelement are all subjected to the acceleration time history recorded in the Earthquake of the Imperial Valley at the El Centro Array station rescaled to a PGA=0.1g. The time history responses of the superstructure and the foundation interface DOFs are compared for the complete FEM simulation and the proposed inelastic LP method. The vertical component of the earthquake motion is neglected. Integration of the equilibrium equation has been performed using a Newmark-type integration scheme. The time history results are depicted in Figures 22 and 23.

From the comparison of the foundation response on the three different approaches, it can be observed that both proposed method M.1 and M.2 are adequately emulating the targeted system behavior. The efficiency of the M.2 method can be explained by the fact that the higher frequency content of the earthquake excitation is filtered out by the superstructure's transfer function, and as stated in 6.2 the simplified method M.2 has adequate results mainly for excitation's with low predominant frequencies. The static macroelement on the other hand is observed to misrepresent the foundation behavior on both rotation and horizontal displacement.

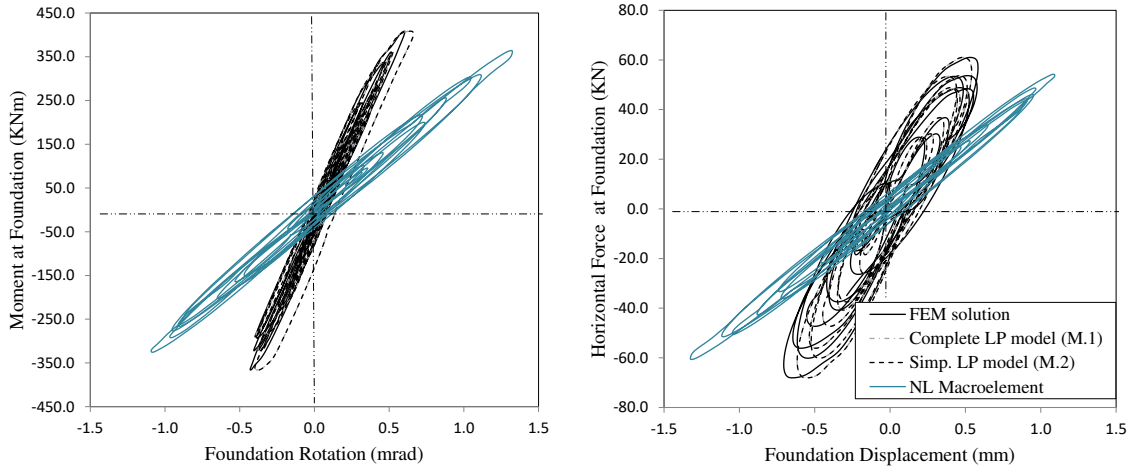

Figure 22. (a) foundation rotation to moment relation (b) foundation horizontal displacement to force relation for the FEM and the reduced model approaches

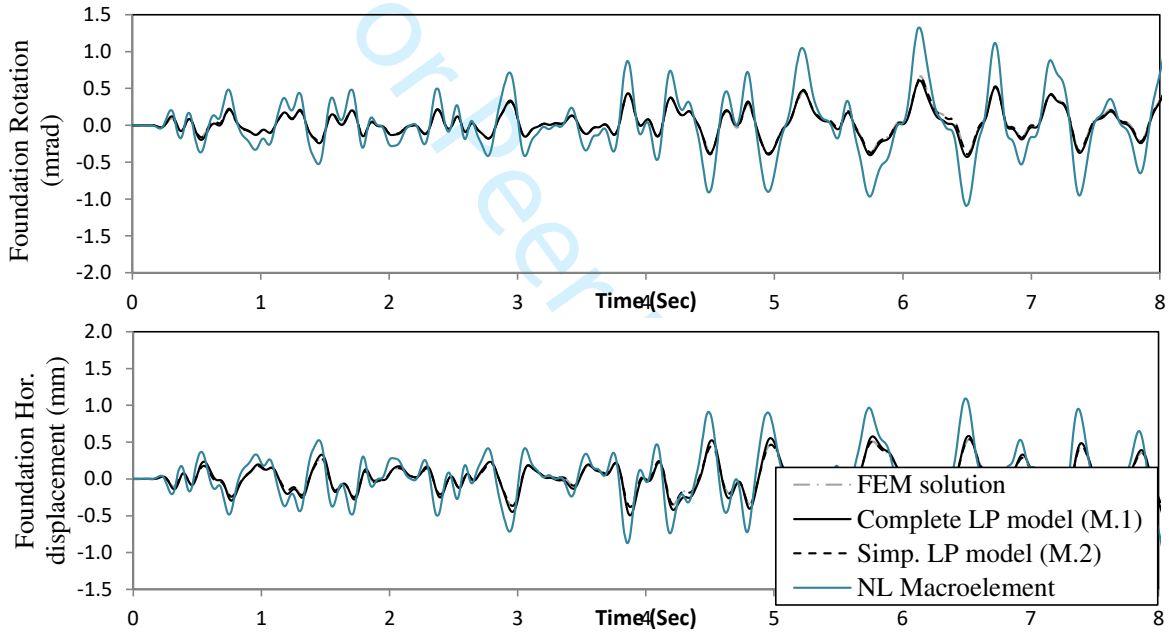

Figure 23. Time history results of the (a) foundation rotation (b)foundation horizontal displacement for the FEM and the reduced model approaches

7. CONCLUSIONS

A new dynamic macroelement method has been developed in the current paper, capable of accurately emulating the inelastic dynamic behaviour of the soil-foundation system. In contrast to methods presented in the existing literature, which either address the system's inelasticity through a frequency independent macroelement or match the dynamic impedance using a dynamic LP model, the proposed intensity- and frequency-dependent lumped parameter model (M.1) copes with the frequency depended properties of the soil-foundation system within a breadth of intensities by means of the expansion of the LP model framework to inelastic dynamic systems. The procedure is numerically verified in dynamic excitations by comparing a refined FE model, the proposed M.1 method, a simplified version of the M.1 approach (M.2) and a sole macroelement. Even though the results are herein limited to simplified soil foundation systems, they demonstrate the efficiency of the proposed frequency- and intensity-dependent LP model (M.1) for the purpose of SSI analyses. Additionally, the simplified approach M.2 was found to be an accurate enough substitute of the complete method M.1 under the conditions of low divergence of the system's impedance functions along the increase of loading intensity. Future work is essential to the expansion of the proposed method for the case of more complex soil-foundation systems.

ACKNOWLEDGEMENTS

This work was supported by the H2020 Framework Programme of the European Commission, under the H2020-MSCA-RISE-2015-691213-Exchange-Risk grant (Experimental & Computational Hybrid Assessment of Natural Gas Pipelines Exposed to Seismic Risk). This support is gratefully acknowledged.

REFERENCES

1. Mylonakis G, Gazetas G. Seismic Soil-Structure Interaction: Beneficial or Detrimental? *Journal of Earthquake Engineering* 2000; **4**(3): 277–301. DOI: 10.1080/13632460009350372.
2. Kwon O, Elnashai A. Seismic Analysis of Meloland Road Overcrossing Using Multiplatform Simulation Software Including SSI. *Journal of Structural Engineering* 2008; **134**(4): 651–660. DOI: 10.1061/(ASCE)0733-9445(2008)134:4(651).
3. Mackie KR, Lu J, Elgamal A. Performance-based earthquake assessment of bridge systems including ground-foundation interaction. *Soil Dynamics and Earthquake Engineering* 2012; **42**: 184–196. DOI: 10.1016/j.soildyn.2012.05.023.
4. Elgamal A, Yan L, Yang Z, Conte JP. Three-Dimensional Seismic Response of Humboldt Bay Bridge-Foundation-Ground System. *Journal of Structural Engineering* 2008; **134**(July): 1165–1176. DOI: 10.1061/(ASCE)0733-9445(2008)134:7(1165).
5. Montrasio L, Nova R. Settlements of shallow foundations on sand: geometrical effects. *Géotechnique* 1997; **47**(1): 49–60. DOI: 10.1680/geot.1997.47.1.49.
6. Chatzigogos CT, Pecker A, Salençon J. Macroelement modeling of shallow foundations. *Soil Dynamics and Earthquake Engineering* 2009; **29**(5): 765–781. DOI: 10.1016/j.soildyn.2008.08.009.
7. Salciarini D, Tamagnini C. A hypoplastic macroelement model for shallow foundations under monotonic and cyclic loads. *Acta Geotechnica* 2009; **4**(3): 163–176. DOI: 10.1007/s11440-009-0087-2.
8. Li Z, Kotronis P, Escoffier S, Tamagnini C. A hypoplastic macroelement for single vertical piles in sand subject to three-dimensional loading conditions. *Acta Geotechnica* 2016; **11**(2): 373–390. DOI: 10.1007/s11440-015-0415-7.
9. Cremer C, Pecker A, Davenne L. Cyclic macro-element for soil-structure interaction: Material and geometrical non-linearities. *International Journal for Numerical and Analytical Methods in Geomechanics* 2001; **25**(13): 1257–1284. DOI: 10.1002/nag.175.
10. Cremer C, Pecker A, Davenne L. *Modelling of nonlinear dynamic behaviour of a shallow strip foundation with macro-element*. vol. 6. 2002. DOI: 10.1080/13632460209350414.
11. Gajan S, Kutter BL. Contact Interface Model for Shallow Foundations Subjected to Combined Cyclic Loading. *Journal of Geotechnical and Geoenvironmental Engineering* 2009; **135**(3): 407–419. DOI: 10.1061/(ASCE)1090-0241(2009)135:3(407).
12. Lesgidis N, Sextos A, Kwon O. Influence of frequency-dependent soil-structure interaction on the fragility of R/C bridges. *Earthquake Engineering & Structural Dynamics* 2017; **46**(1): 139–158. DOI: 10.1002/eqe.2778.
13. Chai S hyeon, Ghaemmaghami AR, Kwon O. Numerical modelling method for inelastic and frequency-dependent behavior of shallow foundations. *Soil Dynamics and Earthquake Engineering* 2017; **92**(August 2016): 377–387. DOI: 10.1016/j.soildyn.2016.10.030.
14. Wolf J. Consistent lumped-parameter models for unbounded soil: Physical representation. *Earthquake Engineering & Structural Dynamics* 1991; **32**(December 1989): 11–32.
15. Paronesso A, Wolf JP. Global lumped-parameter model with physical representation for unbounded medium. *Earthquake Engineering & Structural Dynamics* 1995; **24**(5): 637–654. DOI: 10.1002/eqe.4290240503.
16. Saitoh M. Simple model of frequency-dependent impedance functions in soil-structure interaction using frequency-independent elements. *Journal of Engineering Mechanics* 2007(October): 1101–1114.
17. Lesgidis N, Kwon O, Sextos A. A time-domain seismic SSI analysis method for inelastic bridge structures through the use of a frequency-dependent lumped parameter model. *Earthquake Engineering & Structural Dynamics* 2015: 2573. DOI: 10.1002/eqe.2573.
18. Saitoh M. On the performance of lumped parameter models with gyro-mass elements for the impedance function of a pile-group supporting a single-degree-of-freedom system. *Earthquake Engineering & Structural Dynamics* 2012; **41**(4): 623–641. DOI: 10.1002/eqe.1147.
19. Zadeh L. Optimality and non-scalar-valued performance criteria. *Automatic Control, IEEE Transactions on* 1963; **8**(1): 59–60. DOI: 10.1109/tac.1963.1105511.
20. Coleman TF, Li Y. An Interior Trust Region Approach for Nonlinear Minimization Subject to Bounds. *SIAM Journal on Optimization* 1996; **6**(2): 418–445. DOI: 10.1137/0806023.
21. Lysmer J, Kuhlemeyer R. Finite dynamic model for infinite media. *Journal of the Engineering Mechanics Division* 1969.